INORGANIC CHEMISTRY FRONTIERS

REVIEW

View Article Online
View Journal | View Issue

Cite this: *Inorg. Chem. Front.*, 2024, **11**, 7204

Emerging applications of perovskite oxides in electrochemical reduction of carcinogenic nitrate to ammonia: a recent review

Sadeeq Ullah, [a] Aftab Ahmad, [b] Hefa Cheng, [c] Amin Ullah Jan,[d] Daxiang Cui *[a] and Lu Li*[a]

Ammonia (NH_3) is essential for human endeavors, as around half of the world's food output depends on fertilizers derived from NH_3. Nonetheless, its industrial manufacturing demands substantial energy consumption and releases significant amounts of greenhouse gases, contributing to a variety of environmental concerns. Substantial ventures have been dedicated to creating an eco-friendly and sustainable method for synthesizing ammonia using renewable energy. Catalysts are pivotal in both chemical and electrochemical reactions. Hence, the creation of catalysts exhibiting increased efficiency and durability, obtained from readily accessible Earth materials, holds immense significance. Perovskite oxides, recognized for their significant flexibility in composition and structural design, demonstrate versatile electrocatalytic abilities across a variety of redox reactions. However, a comprehensive review addressing the most recent advancements in the electrochemical reduction of nitrate (NO_3^-) to NH_3 catalyzed by perovskite oxides has been absent until now. This timely review provides readers with a thorough comprehension and up-to-date perspectives on progress made in enhancing the electrocatalytic potential of perovskite oxides in the electrochemical reduction of nitrate (eNO_3RR) to ammonia. We have also explored different strategies capable of enhancing the catalytic efficacy of perovskite oxides. A specific emphasis is placed on understanding how the interplay between perovskite and oxygen vacancies contributes to the improved efficiency of NO_3^- reduction to NH_3. Finally, this review outlines present challenges and upcoming avenues for developing more efficient catalysts based on perovskite compounds.

Received 30th June 2024,
Accepted 8th September 2024

DOI: 10.1039/d4qi01638f

rsc.li/frontiers-inorganic

1. Introduction

Ammonia (NH_3) is a vital global chemical resource, underpinning various industries, including fertilizer production, dyes, and pharmaceuticals. Notably, NH_3 is a carbon-neutral energy vector, making it a key player in sustainable energy storage.[1–5] Currently, large-scale NH_3 production relies on the century-old Haber–Bosch process, requiring harsh conditions (400–500 °C, 150–300 atm.) and Fe-based catalysts.[6–8] The NH_3 production sector, with its significant output and energy-intensive processes, contributes 1–2% to global energy consumption and CO_2 emissions.[3,9,10] Global NH_3 demand is projected to reach 350 million metric tons per year by 2050, driven by population growth and emerging interest in NH_3 as an energy carrier. However, scaling up Haber–Bosch production to meet this demand will require significant capital investment and result in increased CO_2 emissions.[11,12]

Developing sustainable electrochemical conversion methods can significantly reduce CO_2 emissions while producing essential fuels, livestock, pharmaceuticals and chemicals. A key objective is to advance electrocatalytic technologies that convert atmospheric CO_2, water, and nitrogen into valuable products like hydrocarbons, hydrogen, and NH_3, integrated with renewable energy sources (Fig. 1). Electrocatalysts play a crucial role in enhancing reaction rates, selectivity, and efficiency.[13,14] Nevertheless, existing electrocatalysts are inadequate, prompting the need for advanced catalysts with enhanced performance. Combining theoretical and experimental approaches has yielded a framework for understanding catalytic trends, guiding the development of improved catalysts.

[a]*Research Center of Nano Technology and Application Engineering, The First Dongguan Affiliated Hospital, Dongguan Innovation Institute, Guangdong Medical University, Dongguan, 523808, China. E-mail: dxcui@sjtu.edu.cn, lilu2698@gdmu.edu.cn*
[b]*State Key Laboratory of Chemical Resource Engineering, Beijing University of Chemical Technology, No. 15 East Road of North Third Ring, Chao Yang District, Beijing 100029, China*
[c]*MOE Laboratory for Earth Surface Processes, College of Urban and Environmental Sciences, Peking University, Beijing 100871, China*
[d]*Department of Biotechnology, Faculty of Science, Shaheed Benazir Bhutto University Sheringal, Dir Upper, Khyber Pakhtunkhwa 18000, Pakistan*

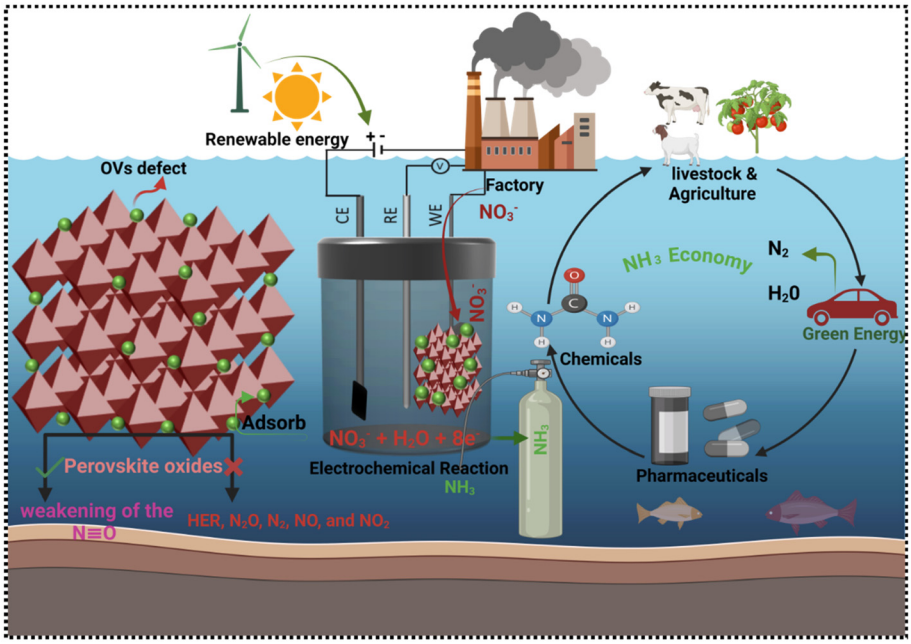

Fig. 1 Electrochemical conversion demonstrates the transformation of diverse molecules into valuable products, all powered by renewable energy sources.

Current investigations target the electrochemical synthesis of NH_3 from nitrogen and NO_3^- precursors, seeking to circumvent the constraints of the Haber–Bosch process through the utilization of renewable electrical energy.[4,8,15,16,17–19] Electrocatalytic ammonia synthesis offers a decentralized, on-site alternative to the Haber–Bosch process, potentially reducing fertilizer costs and achieving carbon neutrality.[20] However, efficient NH_3 production *via* electrochemical methods under mild conditions remains a challenge. Advancements rely on innovative electrode and cell design, urging researchers in chemical engineering, industrial chemistry, and catalysis to focus on these areas. While Haber–Bosch will remain dominant due to global demand, electrochemical synthesis can contribute significantly to decarbonizing NH_3 production.

Despite a decade of research on electrochemical N_2 reduction reaction (NRR) for NH_3 synthesis, the process is hindered by the high energy requirement for breaking the N≡N

Sadeeq Ullah

Dr Sadeeq Ullah received a B.S. degree in Chemistry from the University of Malakand Pakistan in 2014, and an M.S. and a Ph. D. in Materials Science from Beijing University of Chemical Technology, China, in 2018 and 2021. Then, he experienced experimental approaches in the field of electro-catalysis and Biomedical technology concerned with electrochemical methods at Department of the School of Medical Technology in Guangdong Medical University as a postdoctoral position. Currently, he is working at Guangdong Medical University, China, in Bio-Environmental Research and his main research interest is electro-catalyst design for carcinogenic nitrate reduction to ammonia (turning waste to wealth) to create a global sustainable environment.

Lu Li

Prof. Lu Li is currently working in the Laboratory Department of the School of Medical Technology and the Affiliated Dongguan First Hospital of Guangdong Medical University. He earned his doctoral degree from Sun Yat-sen University and conducts research on host–pathogen interactions, with a focus on bacterial resistance and tumor regulation. His work aims to develop sustainable antibacterial strategies without increasing antibiotic use. Professor Li leads several major research projects and has published 18 papers, including 11 SCIE-indexed ones. He has also applied for three national invention patents and received various awards.

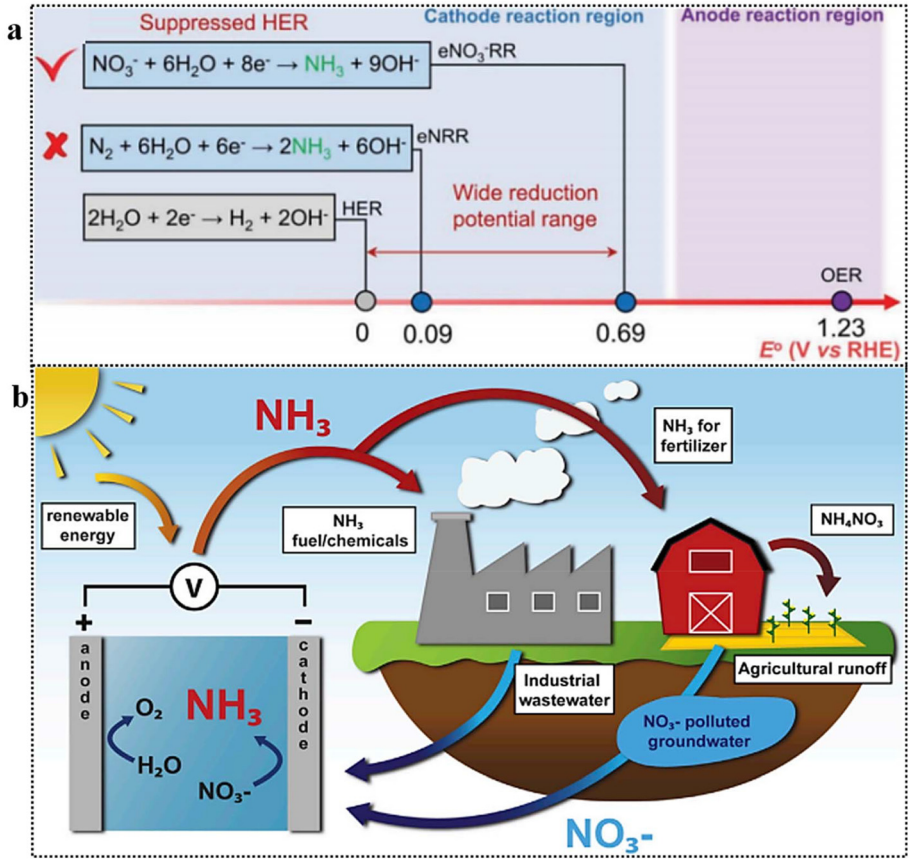

Fig. 2 (a) Comparison of standard reduction potentials for HER, NRR, and NO_3RR. Reproduced from ref. 29 with permission from ACS, copyright 2022 (b) NH_3 synthesis from waste nitrates: conceptual cycle. Reproduced from ref. 36 with permission from Cell Press, copyright 2021.

triple bond (942 kJ mol^{-1}) and the competing hydrogen evolution reaction (HER), which compromises faradaic efficiency (FE) and production rate.[17,21–26,27] The electrochemical reduction of N_2 is impeded by its inherent inertness and sluggish kinetic activity. Although the NRR process ($6H^+/6e^-$) and HER pathway ($2H^+/2e^-$) exhibit comparable redox potentials, the latter predominates due to its more favorable thermodynamics. In stark contrast, the electrochemical reduction of NO_3^- to NH_3 proceeds with a substantially higher reduction potential, facilitating selective NH_3 synthesis while inhibiting HER (Fig. 2a).[28,29] Thus, electrochemical N_2-to-NH_3 conversion faces significant challenges: poor selectivity, low yield, and accurate NH_3 quantification in aqueous media.[30,31] A meta-analysis studies reveals insufficient NH_3 yield rates, suggesting that aqueous NRR methods likely do not produce NH_3 from N_2, emphasizing the need for advanced electrocatalysts in aqueous media.[31]

Conversely, the electrochemical NO_3^- reduction reaction (NO_3RR) presents several benefits as a strategy for low-temperature NH_3 synthesis,[32,33] and the conversion of nitrate, a toxic pollutant in water, into the valuable chemical NH_3 is highly appealing (Fig. 2b).[34,35] Moreover, in terms of energy considerations, the required energy to break the N=O bond in NO_3^- (204 kJ mol^{-1}) is considerably lower compared to N≡N, which has favorable implications for reaction kinetics.[13,36] The presence of NO_x (nitrate and nitrite) in drinking water poses a direct threat to human health.[37] Nitrite (NO_2^-), which is derived from NO_3^-, is a potentially carcinogenic substance that can contribute to the development of various diseases.[38,39]

As a result, ensuring the elimination of both NO_3^- and NO_2^- from water has become crucial for safeguarding public health. Hence, the NO_3RR pathway appears as a favorable approach for renewable NH_3 synthesis, offering the additional benefit of facilitating wastewater denitrification and restoring balance to the disrupted nitrogen cycle.[20,40–44] The success of the electrochemical NO_3RR technique largely hinges on the careful selection of electrode materials. This choice plays a crucial role in minimizing overpotential, enhancing reaction rates, and improving the selectivity towards highly reduced products.[20,45–47] However, the application of NO_3^- reduction reaction has encountered obstacles attributed to the inadequate activity, selectivity, and stability of electrocatalysts. The conversion of NO_3^- to NH_3 entails a complex multi-electron transfer practice, and the competitive nature of the HER assumes critical importance in this regard. Moreover, the NO_3^- to NH_3 reaction typically exhibits a lower potential compared to the HER, leading to the generation of H_2, depletion of

electron donors, and hence, affect selectivity and FE.[48,49] As a result, there is an immediate demand for catalysts that can hinder the formation of N≡N bonds, suppress the HER, and effectively adsorb NO_3^- and other intermediate species. This will facilitate the efficient and selective conversion of NO_3^- to NH_3.

Transition metal oxides (TMOs) have recently emerged as a prominent class of electrocatalysts, garnering substantial interest due to their potential to enhance electrochemical reactions. Recent research has underscored the significance of transition metal oxides (TMOs),[50,51] specifically copper-based compounds, in facilitating the electrochemical conversion of NO_3^- to NH_3 with high selectivity. Copper oxide electrocatalysts have exhibited a unique capability to catalyze this reaction on diverse surfaces, including crystalline and amorphous architectures, thereby demonstrating their utility as versatile nanocatalysts in this field of study.[52–54] The catalytic performance of TMOs is not solely determined by the inherent attributes of metal sites but is also influenced by the presence of oxygen vacancies (OVs), which are commonly found in these oxides.[55–57] The presence of OVs has been observed to influence the manipulation of electronic structures and the modulation of the adsorption behavior of reaction intermediates.[58,59] Furthermore, it has been demonstrated that OVs exhibit effective binding of NO_3^- ions, thereby preventing the formation of byproducts during electrocatalysis.[60] Similarly, perovskite oxide, a versatile class of advanced functional materials, has gained significant attention for its exceptional catalytic activity, composition, conductivity, and tunable structure, making it suitable for catalyzing various reactions.[61–66] Unlike conventional metal oxides, perovskite oxides possess a distinctive structure allowing specific metal cations to adopt mixed valence states,[67,68] leading to the generation of OVs within the material. Furthermore, the perovskite oxide demonstrates exceptional structural stability and offers the flexibility to substitute A-site and B-site moieties with desired elements of different valence states.[69–72] As a result, precise control over the oxidation state of the B-site cation and the concentration of OVs is achievable through the introduction of the desired dopant. This convenient and feasible approach facilitates the association between physicochemical attributes and the catalytic proficiency of the materials.[63,73,74] The combination of the intrinsic catalytic properties of perovskites with the presence of OVs allows these materials to function as efficient electrocatalysts for the reduction of NO_3^- to NH_3.

Taking into consideration the catalytic performance of perovskites and OVs, we have undertaken an effort to elucidate their significance in the electrochemical conversion of NO_3^- pollutants into valuable products, specifically NH_3. Although the catalytic efficacy of perovskite oxides has been thoroughly explored across various scientific fields, a comprehensive review paper outlining their role as electrocatalysts for the efficient conversion of NO_3^- to NH_3 has not been published, as evidenced by our literature survey. In this up-to-date review, we provide a comprehensive summary of the recent developments in the electrochemical conversion of NO_3^- to NH_3, focusing on the utilization of various perovskite oxide compositions and properties.

1.1. Nitrate in drinking water is a global issue

NO_3^- is commonly recognized as a water pollutant and an unwanted residue from fertilizer usage, contributing to water contamination through excessive fertilizer application, biomass degradation, fossil fuel consumption, and industrial discharges.[75] Given NO_3^- high solubility in water, human exposure primarily occurs through various routes such as drinking water and food uptake. Additionally, global climate change has emerged as a significant concern in recent times, posing a threat to human health by disrupting hydrobiological systems and degrading water quality due to elevated NO_3^- concentrations. Extensive epidemiological studies have revealed that reduced water availability and heightened NO_3^- concentrations correlate with an increased risk of various medical conditions, including cancer, thyroid disease, adverse birth outcomes, and other health implications associated with NO_3^- exposure in drinking water.[76] Consequently, NO_3^- contamination in groundwater is a worldwide concern that has garnered significant attention from researchers over the years. Human actions, including the production and application of nitrogen fertilizers and the combustion of fossil fuels, have doubled the natural rate of nitrogen deposition on land. NO_3^- pollution poses a significant threat as it can pollute surrounding waters, serving as a harmful pollutant that directly impacts human health.

Overexposure to nitrate/nitrite in water and food can pose risks to human health by (1) contributing to the formation of *N*-nitroso compounds internally, which are carcinogenic in animal studies; (2) potentially leading to methemoglobinemia; and (3) at elevated levels, competitively inhibiting iodine absorption and causing alterations in thyroid function. Furthermore, high NO_3^- concentrations in drinking water can negatively affect children and infants, resulting in the potentially life-threatening condition of methemoglobinemia, as well as adverse outcomes during pregnancy.[77]

1.2. Effects of nitrate/nitrites on human health

1.2.1. Gastric cancer. Although NO_3^- exhibits minimal cytotoxicity, its enzymatic reduction to NO_3^- by bacterial flora raises concerns regarding the formation of carcinogenic *N*-nitrosamines[78] (Fig. 3a). This process can occur through two primary pathways: (i) the acidic gastric milieu, wherein nitrous acid (HNO_2) and reactive nitrogen oxides (N_2O_3 and N_2O_4) are generated, and (ii) bacterial colonization in low-acidity environments, where *N*-nitroso compounds are formed at neutral pH *via* enzymatic catalysis (Fig. 3). The precise mechanism underlying this phenomenon remains uncertain, but it is speculated to involve bacterial nitrite reductase, leading to increased production of NO or related compounds. It's important to note that NO itself does not function as a direct nitrosating agent. However, in the presence of oxygen, NO can oxidize to form NO_2, which, in equilibrium with N_2O_3 and

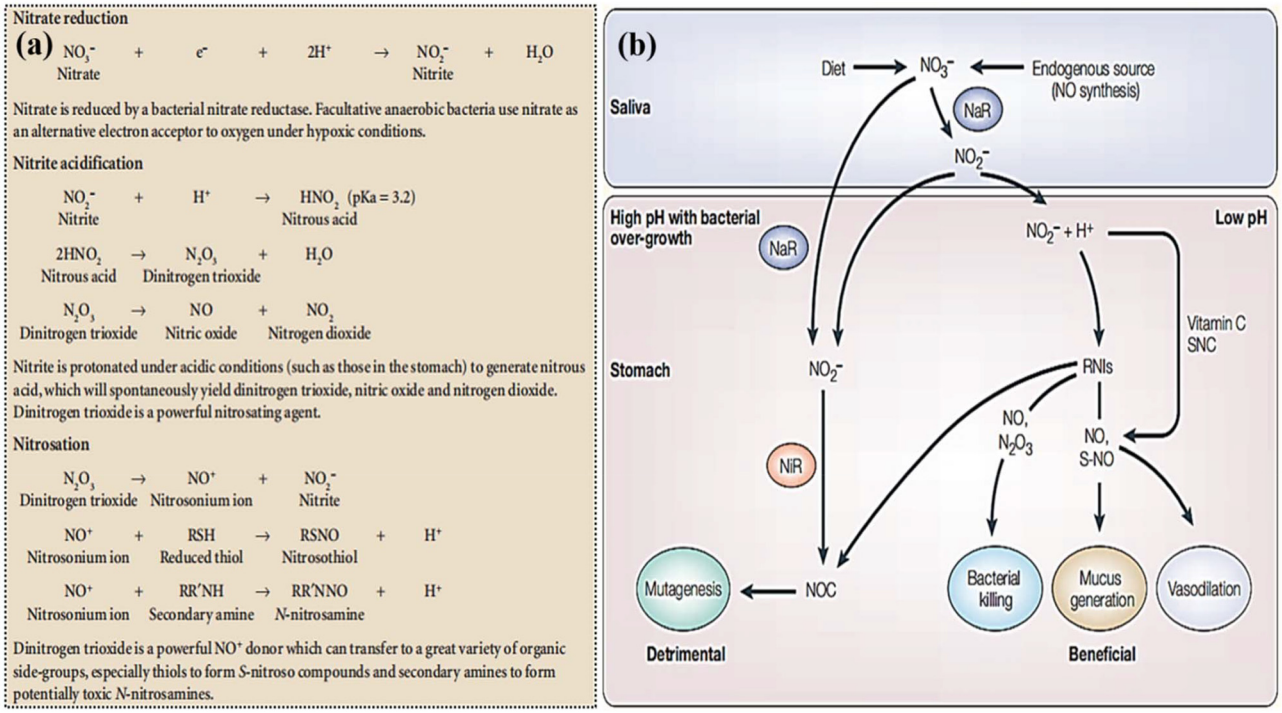

Fig. 3 Complex chemical reactions produce nitrosating agents and nitroso compounds from NO_3^- reduction. Reproduced from ref. 37 with permission from nature, copyright 2004. (b) Hypothesized gastrointestinal effects of nitrite are shown. Blue indicates bacterial nitrate reductases (NaR) and red indicates nitrite reductases (NiR). NOC stands for *N*-nitroso compounds, RNIs for reactive nitrogen intermediates, SNC for thiocyanate, and *S*-NO for *S*-nitrosothiols. Reproduced from ref. 37 with permission from nature, copyright 2004.

N_2O_4, can react with secondary amines at physiological pH to produce *N*-nitroso compounds.[37,79,80] The use of antioxidant compounds like Vitamin C and E, among others, may support and inhibit endogenous nitrosation.[81] Vitamin C, for instance, has been demonstrated to impede the formation of *N*-nitroso compounds by rapidly converting nitrous acid to nitric oxide and generating dehydroascorbic acid.[82]

1.2.2. Bladder cancer. During normal physiological conditions, NO_3^- from both dietary sources and those produced within the body is excreted through urine. In the absence of urinary tract infections, the naturally sterile nature of urine avoids additional reduction to NO_3^-. But, when urinary tract infections are present, bacteria can catalyze the alteration of NO_3^- to nitrite, leading to substantial nitrite accumulation. Specifically, during infection conditions triggered by *Schistosoma haematobium*, the risk of bladder cancer is substantial, with *N*-nitrosamines suggested to have a significant role in cancer development.[83,84] The invading bacteria possess the ability to convert urinary NO_3^- to nitrite, thereby facilitating the production of elevated levels of *N*-nitrosamines. Some research suggests that nitrosamine synthesis in the bladder may be enhanced by increased local endogenous nitric oxide (NO) generation after long-term parasite infection.[85]

1.3. Methemoglobinemia

Infants possess distinct physiological characteristics that elevate their susceptibility to methemoglobinemia. They consume a higher volume of water relative with relation to the weight of adults and children, exhibit reduced activity of NADH cytochrome b5 reductase responsible for converting methemoglobin to hemoglobin, and also have more fetal hemoglobin, which converts more easily to methemoglobin.[86] Infants exposed to elevated concentrations of NO_3^- may experience this life-threatening condition known as methemoglobinemia. Following the consumption of the substance, bacteria that are present in the oral cavity and stomach of the new catalyze the transformation of NO_3^- into nitrite. Subsequently, this nitrite binds to hemoglobin, oxidizing it and leading to the formation of methemoglobin, consequently reducing the blood's capacity to transport oxygen. The primary cause of methemoglobinemia in infants, as well as enteric fevers, is the consumption of water, food, and medications containing high levels of NO_3^-.[87] Evidence from multiple reports indicates a direct correlation between the feeding of NO_3^--rich water and the onset of methemoglobinemia in multiple regions.[77,86,88]

1.4. Thyroid dysfunction

Other pathways such as the thyroid gland's suppression of iodine uptake and changes in thyroid function are further potential routes of damage caused by NO_3^-. NO_3^- can interfere with the sodium iodide symporter by inhibiting the Na^+/K^+ ATPase, thus impeding the thyroid gland's normal function. As a consequence of this disturbance, irregularities in the production of thyroid hormones, such as triiodothyronine (T_3)

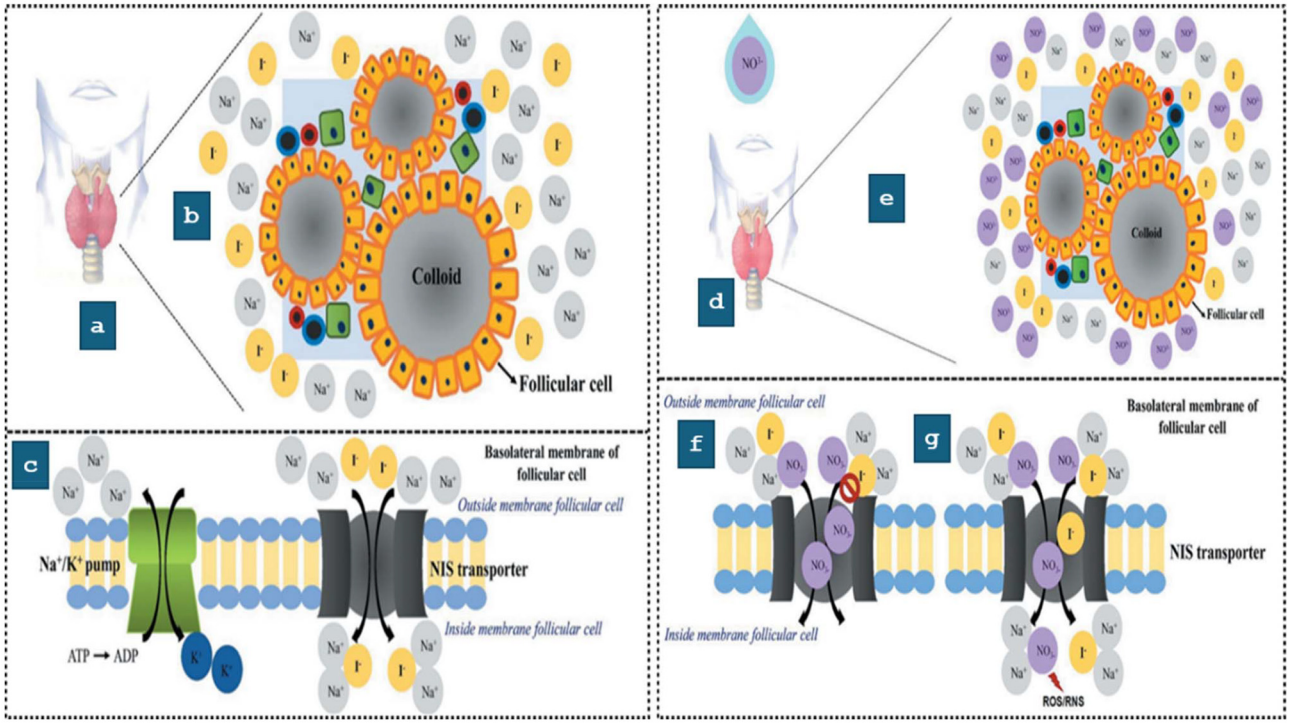

Fig. 4 A typical example of the thyroid gland in its normal functioning condition: (a) illustration of the thyroid gland. (b) The NO_3^- free follicular microenvironment. (c) Under normal circumstances, the Na^+/I^- Symporter (NIS) in the basolateral thyroid follicles (TF) transports iodine actively, thereby enabling the synthesis of thyroid hormones, during the presence of NO_3^- the operational status of the thyroid gland (d) thyroid gland. (e) In the presence of NO_3^-, the follicular microenvironment. (f) The presence of NO_3^- may block the Na^+/I^- Symporter (NIS), disrupting iodine transfer to thyroid follicles (TF) and limiting thyroid hormone production. (g) Proposed interruption of the NIS-mediated active transport pathway for iodine to the TF, reducing absorption and allowing NO_3^- channel. This reduces thyroid hormone production and may produce nitric oxide and ROS/RNS. Reproduced from ref. 95 with permission from Taylor & Francis, copyright 2022.

and thyroxine (T_4) may occur, which can result in iodine deficiency and affect the pituitary gland's function as well.[89,90] For proper function, the thyroid gland (TG) necessitates normal morphology and undergoes typical biochemical processes. This process entails the internalization of iodine *via* the sodium/iodide symporters (NISs)-facilitated absorption of iodide.[91] This normal functioning of the TG in the absence of NO_3^- is depicted in (Fig. 4). The normal operation of the thyroid gland (TG) can be upset by either of two potential disruption developments, as illustrated in Fig. 4(d and e). In the first scenario, elevated NO_3^- levels reach the TG through the consumption of contaminated water, impacting iodine intake by blocking the Na^+/I^- symporters (NISs) (Fig. 4(c)). In the second scenario, NO_3^- interferes with the NISs (Fig. 4(g)). Nitrate-mediated inhibition of iodide uptake has been associated with thyroid cancer. Insufficient iodine availability reduces the production of T_3 and T_4, leading to the release of thyroid-stimulating hormone (TSH). Studies in animal models have demonstrated that increased levels of TSH contribute to thyroid cancer.[92] Additionally, nitroso compounds generated from NO_3^- reduction have been linked to thyroid carcinogenesis. Researchers found a clear correlation between NO_3^- consumption and the occurrence of thyroid cancer in the Iowa Women's Health Study and the NIH-AARP Diet and Health project.[93,94] Researchers found that the risk of thyroid cancer was significantly raised in correlation with the use of NO_3^- in both food and water.

1.5. Effect on pregnancy outcomes

Elevated NO_3^- levels in drinking water are associated with increased risk of adverse pregnancy outcomes, including neonatal mortality, congenital abnormalities, intrauterine growth restriction, and premature birth. The proposed mechanism involves nitrate reduction to nitrite, which oxidizes hemoglobin to methemoglobin, impairing oxygen transport and reducing fetal oxygen supply. Fetal plasma NO_3^- levels may exceed maternal levels due to transplacental transfer, exacerbating the risk of nitrate-induced adverse birth outcomes.[76,96,97] Newborns have limited antioxidant defenses, making them vulnerable to oxidative and nitrosative stress. Antioxidants present in food sources may partially mitigate these effects, but drinking water lacks antioxidants, potentially making NO_3^- consumption more hazardous. Alternative mechanisms, including *N*-nitroso compound formation and disruptions in thyroid and endocrine function, have been proposed to explain nitrate's potential impact on reproductive health.[98,99] Recent review papers have extensively examined

the suggested study on NO_3^- in drinking water and harmful reproductive and newborn outcomes.[76,100]

In summary, excessive NO_3^- levels in water pose a substantial health hazard, warranting prompt mitigation strategies. The electrochemical reduction of NO_3^- to NH_3 *via* catalytic processes has emerged as a viable solution, with nanoscale catalysts, particularly perovskite oxides, exhibiting notable efficacy. The exceptional efficiency of these materials in facilitating the electrochemical conversion of NO_3^- pollutants to valuable NH_3 has garnered significant research attention. This review provides a comprehensive overview of the recent advancements in the application of perovskite oxides for electrochemical NO_3^- reduction to NH_3.

2. Structural importance of perovskites in catalysis

Mixed metal oxides form the foundation for the majority of catalysts utilized in today's chemical industry. The focal point of research in the realm of heterogeneous catalysis revolves around creating custom-designed mixed oxides with the capability to execute intricate tasks. To accomplish complex catalytic reactions, it is necessary to employ a multifunctional catalyst that possesses suitable properties in terms of morphological characteristics, exposed surface, and solid-state. Perovskite-type oxides continue to maintain prominence among the various types of mixed metal oxides. These substances can be described by the overall composition ABO_3, where A ion (larger cations) encompass rare earth, alkali/alkaline earth, and other sizable ions (Pb^{2+} and Bi^{3+}) that suitably occupy the dodecahedral position within the structure. The B ions refer to transition-metal cations (3d, 4d, and 5d) encircled by six oxygen atoms that occupy the octahedral positions.[101,102] While the perovskite structure is primarily associated with oxides, it is important to acknowledge that certain carbides, nitrides, halides, and hydrides also adopt this crystalline arrangement, although to a lesser extent. Double perovskite oxides, denoted as $AA'B_2O_6$ or $A_2BB'O_6$, can be synthesized by introducing two different varieties of A-site or B-site cations (Fig. 5a). Although there are variations in the structures, the presence of $[BO_6]$ octahedra is a consistent feature, and it is currently understood that B-site cations play a vital role in electrocatalysis.[103]

Understanding the connection between the catalytic characteristics and solid-state properties of inorganic compounds is crucial for the purposeful development and customization of effective catalysts, rather than relying solely on trial and error approaches. To explore these connections, having access to a diverse range of isostructural compounds that exhibit flexibility and adaptability provides significant advantages. The structure and composition of ABO_3 perovskite compounds offer a simplified approach to address the intricate task of establishing crucial correlations. They play a vital role in this aspect. Typically, the A ions exhibit minimal catalytic activity, while the active transition metal ions located at the B site maintain an appropriate separation from one another (approximately 4 angstroms). This spatial arrangement ensures that a gas molecule interacts with a singular site.[102] Furthermore, even when dealing with a solitary active metal B center, there exists the opportunity to modify its valence and various physical properties by selecting the "modifying" A moiety. Perovskite oxide has gained recognition as a groundbreaking catalyst material, primarily due to its outstanding catalytic activity, adaptable structure, and composition.[104] Unlike other metal oxides, perovskite oxides exhibit a unique structure that allows specific metal cations to assume unconventional or mixed valence states.[65] Furthermore, the enhanced physiochemical attributes of ABO_3, including aspects like structural stability, surface area, electronic properties, and reducibility, which stem from modifications in ABO_3 structure and composition, play a crucial role in facilitating catalytic redox reactions across various catalytic pathways.[105] Perovskite materials possess the capacity to withstand significant levels of partial substitution and non-stoichiometry without compromising their inherent perovskite structure (Fig. 5b).[106] This characteristic allows metal ions with different valences to replace both A and B ions within the structure, resulting in the occurrence of non-stoichiometric OVs. In metal oxides, the crystal structure has a prominent impact on the electronic levels, leading to the creation of an electrostatic potential specific to each distinct crystallographic site, as depicted in 'Madelung Potential' shown in (Fig. 5c).[107] As per the molecular orbital theory (MOT), the octahedral spatiality in perovskites plays a significant role in catalyzing reactions.[68,107] The electron energy of free M^+ ions within perovskite oxides and oxygen anions is influenced by their ionization energy in a vacuum. However, once these ions occupy the crystallographic sites of perovskite oxides, a notable phenomenon arises. Oxygen anions, when surrounded by cations, exert an attractive effect on electrons. In contrast, B-site cations, when encompassed by oxygen anions, give rise to a repulsive effect on electrons. As a consequence, these interactions lead to a modification in the electron energies of cation (M^{n+}) and anion (O^{2-}), ultimately giving rise to the formation of an inverted Madelung potential (Fig. 5c1). Because of the significant similarity in orbital energies and spatial overlap between the O 2p and metal d orbitals, hybridization occurs, resulting in the formation of two bonding, two antibonding, and one non-bonding orbital in the crystal field (Fig. 5c2). The perovskites' M–O (metal–oxygen) bonds exhibit a blend of ionic and covalent attributes[108] due to the resemblance in covalency (energy levels) and the hybridization (spatial alignment) of metal 3d orbitals with O 2p states. This interplay has been demonstrated to impact catalytic activities.[109–111] By replacing the B-site with a more electronegative element or oxidizing the B-site element, it is possible to increase the covalency and hybridization of the M–O bond.[112,113] This results in a closer alignment between the metal 3d states and the O 2p states, leading to a shift in the Fermi level towards the O 2p states (Fig. 5d). As a consequence, the energy required for generating O vacancies is reduced,[114] ultimately enhancing the electronic

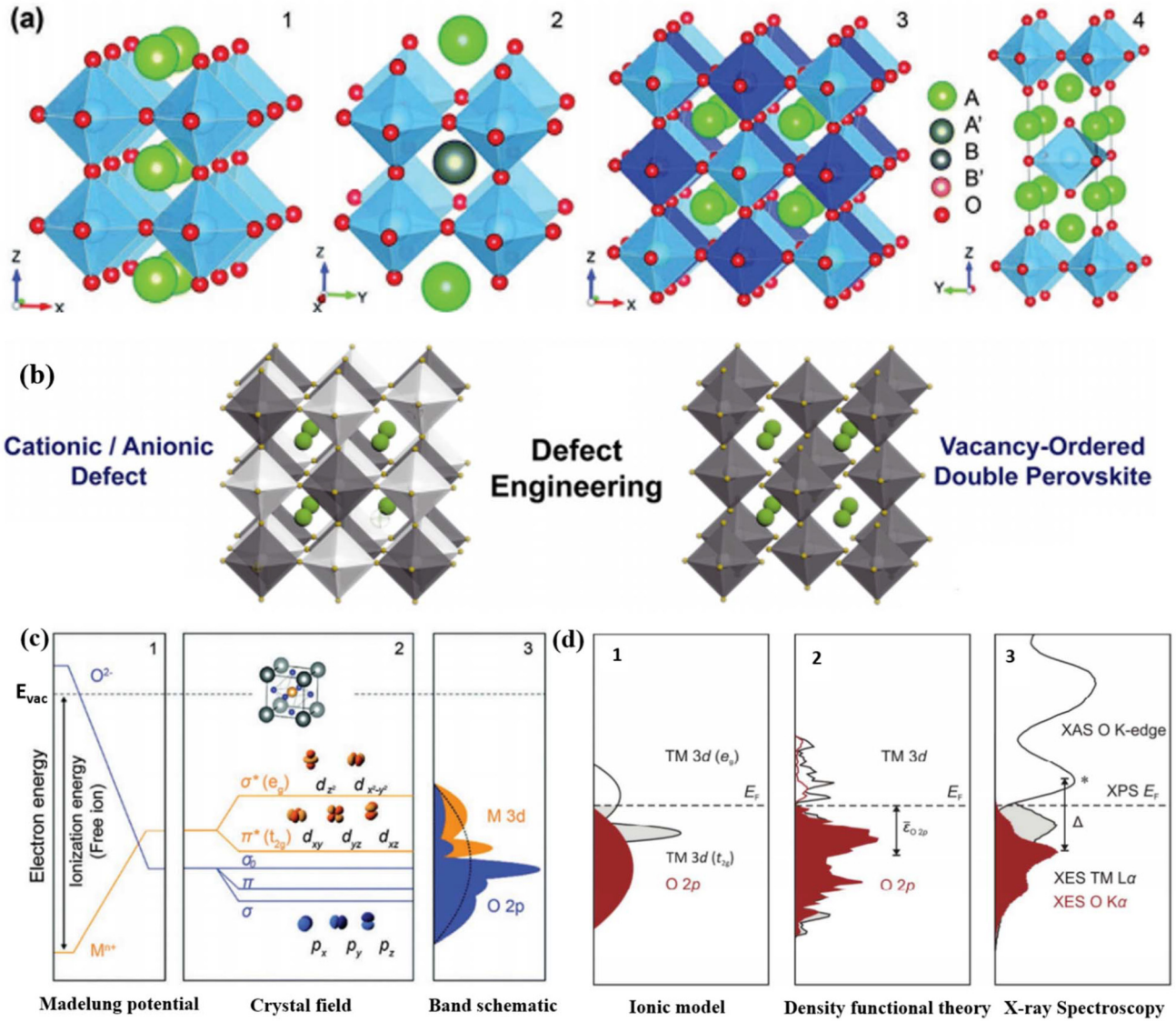

Fig. 5 (a) Crystal organizations of (1) the perfect ABO_3 perovskite oxide, (2 and 3) double perovskite oxide (A and B-site ordered), and (4) Ruddlesden–Popper type perovskite oxide (An + $1BnO_3n$ + 1). Reproduced from ref. 65 with permission from RSC, copyright 2020. (b) Defect sites (A-, B-, or X-site), and V_O-ordered double perovskite halide. Reproduced from ref. 106 with permission from Cell Press, copyright 2019, (c) oxide band structure (unit cell inset): (1) energy profile and the on-site Madelung potential of ions, illustrating the shifts of energies in the crystal lattice (energy of free vacuum, E_{vac}, in dashed lines); (2) asymmetric covalent hybridization amongst orbitals (M 3d and O 2p) generates σ- and π-bonding and antibonding orbitals; (3) illustrating the one-electron band structure displaying shapes with partial transition metal (orange) and oxygen attributes (blue), respectively, with the three oxygen bands often depicted as a unified broad band designated by the dashed curvature. Reproduced from ref. 107 with permission from RSC, copyright 2015, (d) demonstrations of electronic assembly near the Fermi level. Partial density of states of TM and O based on (1) the ionic model, (2) DFT, and (3) X-ray spectroscopy of $LaCoO_3$. Panel (2) schematically illustrates the O 2p-band location relative to the Fermi level. Reproduced from ref. 121 with permission from RSC, copyright 2017.

and/or ion conduction capabilities of perovskites. Furthermore, perovskite oxides possess significant benefits when compared to other oxides, primarily due to their versatile electronic structure and flexible composition. By varying the arrangement of metal ions in the A and B sites, perovskite oxides can serve various functions such as conducting oxygen or protons, exhibiting mixed ionic-electronic conductivity, and therefore acting as versatile catalysts in multiple reactions.[68,115–120]

3. Strategies to improve the catalytic performance

To boost the efficiency of an electrocatalyst system, there are generally two primary approaches. The first approach focuses on augmenting the number of active sites on a specific electrode, which can be accomplished by increasing the loading or improving the catalyst structure to expose a greater number of

active sites per unit of catalyst. The second approach involves enhancing the intrinsic activity (electronic structure of catalysts) of each active site.[122] These strategies can be pursued simultaneously, as they are not mutually exclusive, resulting in the greatest possible improvements in activity. However, it is crucial to recognize that there are practical constraints regarding the quantity of catalyst material that can be loaded onto an electrode, as it may negatively impact essential processes like charge and mass transport. Conversely, augmenting the intrinsic activity directly enhances electrode activity while mitigating transport challenges caused by high catalyst loadings. With improved intrinsic activity, the catalyst loading can be reduced, resulting in cost savings on catalyst materials.[13] By employing techniques like elemental doping and defect engineering, the electronic structure, an intrinsic property of the designed electrode material, can be effectively controlled. The catalyst selectivity is largely governed by the electronic arrangement of different metals, particularly in terms of the binding strengths of nitrogen and oxygen, and the coverage of *H on these materials.[123]

3.1. Oxygen vacancy (OV)

Defect engineering demonstrates its effectiveness not only in enhancing intrinsic activity but also in mitigating competing side reactions, which include HER and the generation of other byproducts such as N_2O, N_2, NO, and NO_2. Vacant sites can modulate the electronic structure of catalysts and optimize the reaction pathway, resulting in improved overall efficiency.[55,124–126] Referring to a recent study on V_O in Fe_2O_3 as a reference,[127] it has been verified that OV exerts beneficial effects on charge transfer and catalytic activities, while simultaneously hindering the quenching of the generated charges at the catalyst/interface (Fig. 6a). Similarly, the presence of OVs in the $Bi/Bi_2O_{2-x}CO_3$ catalyst facilitates the efficient transfer of photo-induced electrons, leading to the activation of H_2O_2 production. Consequently, this mechanism greatly boosts the oxidation of NO_x.[128] Additionally, the ample OVs within the $Bi/Bi_2O_{2-x}CO_3$ catalyst serve as a valuable source of active and adsorption sites, contributing to the enhancement of visible light activity in the tested photocatalyst (Fig. 6b). The presence of metal cations along with adjacent OVs creates unsaturated active sites capable of adsorbing and weakening the N≡O bonds, thereby facilitating the reduction of NO_3^-.[129] In their study, Jia *et al.* demonstrated that the TiO_{2-x}, led to the weakening of the N≡O bond and subsequently reducing thermodynamic barriers.[130] Liu *et al.*[131] discovered that $LaCoO_3$ with a high concentration of oxygen vacancies demonstrated a substantially higher NH_3 yield rate compared to pristine $LaCoO_3$. The NH_3 yield rate for $LaCoO_3$ with abundant oxygen vacancies was 2.8 times greater than that of pristine $LaCoO_3$. Density functional theory (DFT) calculations supported these findings by indicating that OVs facilitate the formation of electron-rich active sites, leading to the weakening of the triple bond with subsequent activation of N_2 molecules. The introduction of metal atom doping in catalysts offers the potential to reduce the energy barrier of the reaction,[132,133] leading to the generation of OVs.[134,135] This, in turn, enhances the performance of the catalysts. As per reported findings, the induction of OVs in Fe-doped TiO_2 and Cu/CuO_x causes charge redistribution, resulting in the creation of multiple active sites for NO_3^- adsorption and subsequent reduction.[136] According to Fenglin Zhao *et al.*[137] for the HER, the energy barrier for hydrogen generation is higher on Co_3O_4–2Ov (1.15 eV) compared to Co_3O_4–1Ov (0.83 eV) and Co_3O_4 (0.66 eV). Indicates that HER is more challenging on Co_3O_4–2Ov than on the other two materials. The availability of OVs on Co_3O_4–2Ov seems to inhibit HER. Similarly, the HER free energy calculations (Fig. 6e) show a quite different trend. Introducing 1 oxygen vacancy (OV) reduces the free energy barrier from +0.41 eV (with no OV) to +0.04 eV (with 1 OV). However, increasing the OV beyond 1 OV raises the free energy of H* from +0.41 eV (no OV) to −0.6 eV (2 OVs) and −0.68 eV (3 OVs). The DFT results suggest that while a low concentration of OVs can enhance HER and suppress NO_3RR, interestingly, a higher concentration of OVs (beyond 1 OV) makes HER more challenging. Therefore, these theoretical findings indicate that CuO nanomaterials with an optimal level of defects can serve as effective catalysts for high-yield and selective NO_3RR. Moreover, OVs play a critical role in impeding proton reduction, effectively preventing the HER (Fig. 6c–e).[138,139]

The catalytic performance in perovskite-based catalysis relies significantly on the band gap between the d-band and Op band centers. Achieving proximity between the d-band and the Fermi level holds vital importance to effectively catalyze a chemical reaction. Scientific evidence supports that the presence of OVs in perovskite catalysts has a substantial effect on reducing the band gap, thereby bringing the metal d-band closer to the Fermi level. Consequently, this facilitates faster reaction kinetics, leading to improved catalytic performance (Fig. 7a and b).[140] Numerous factors play a role in influencing the center of the O 2p-band within perovskite oxides. These factors encompass defects,[65] strain, and the oxidation state of B-site cations,[68,141,142] experienced by the perovskite oxides. To illustrate, the presence of OVs can lead to an upward shift in the Fermi level, enabling the adjustment of the O 2p-band center's position (depicted in Fig. 7c, left panel), while also generating electron holes that enhance charge transfer and electron conduction. Furthermore, OVs can alter both the configuration of surface elements, impacting the adsorption of intermediates, and the crystal structure, subsequently influencing the B–O interaction within perovskite oxides and thus fine-tuning catalytic activity.[65] The process of oxidizing the B-site (from B^{n+} to B^{n+1}) results in a reduction of the M 3d-band's energy level, consequently causing the Fermi level to shift downward towards the O 2p-band. This shift facilitates an augmentation in the degree of overlap (hybridization) between these bands (as depicted in Fig. 7c, right panel).

Moreover, based on theoretical calculations, the presence of OVs has been shown to enhance the interaction between reactants and reduce the energy barrier for the rate-determining step on the perovskite surface (Fig. 7d).[143] These findings hold promise in offering practical guidance for activating catalyst

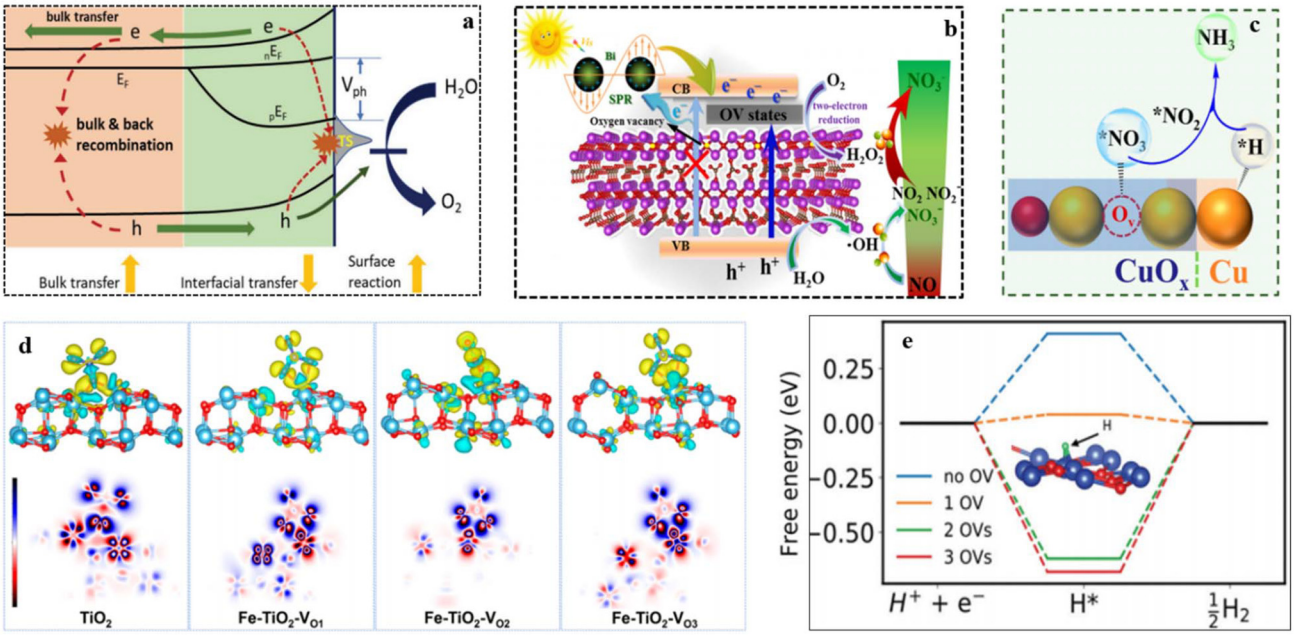

Fig. 6 (a) The mechanism of OV influence on photoelectrochemical water oxidation on Fe_2O_3. Reproduced from ref. 127 with permission from Wiley, copyright 2019, (b) schematic illustration of charge transfer in the $Bi/Bi_2O_{2-x}CO_3$ system and the possible mechanism of photocatalysis. Reproduced from ref. 128 with permission from Elsevier, copyright 2019, (c) schematic illustration of the electrochemical NO_3^--to-NH_3 route on Cu/CuO_x/CF catalyst. Reproduce from ref. 136 with permission from ACS, copyright 2022, (d) differential electron density mappings (TiO_2 and Fe-doped TiO_2) following NO_3^- adsorption. The red, blue, royal blue, and green domains represent O, Ti, N, and Fe atoms, respectively. Depletion and accumulation of electron density are denoted by green and yellow NO_3^- regions, respectively. OVs are indicated by orange dotted regions. Reproduce from ref. 71 with permission from Wiley, copyright 2021. (e) The HER free energy diagram (CuO) with 0, 1, 2, and 3 OVs. Reproduce from ref. 138 with permission from RSC, copyright 2021.

surfaces. Furthermore, empirical evidence has established that the introduction of V_o in the ABO_3 system brings about modifications in various attributes of the perovskite oxide, including crystal reduction, bond dissociation, phase stability, and delocalization. As a result, this instigates an improvement in the physiochemical properties and application performance of the material (Fig. 7e).[144] Theoretical analyses have also showcased that introducing OVs not only assists in the adsorption and activation of the N_2 molecule but also enhances the reaction pathways by amplifying the interactions between adsorbed species and vacant Fe sites in $LaFeO_3$ (Fig. 7f).[145] From an examination of the structural characteristics of perovskite oxides, it has been established that manipulation of the oxidation state of the cation occupying the B-site, as well as the creation of oxygen vacancies within the lattice framework, can be achieved through the substitution of an external cation.[146] This substitution process preserves the overall matrix structure of the material. Following the insights depicted in (Fig. 7g), which focuses on a perovskite of the ABO_3 type, it is demonstrated that the substitution of an A^{3+} cation with an A'^{2+} cation within the $A^{3+}_{1-x}A'^{2+}_xBO_3$ composition can lead to an elevation in the oxidation state of the B-site cation (from B^{3+} to B^{4+}), or OVs can be induced. Managing the oxidation state of the metal cation on the B-site and regulating the concentration of OVs holds significant significance. This is because the catalytic cycle is intricately tied to the redox characteristics of the B-site metal cation, while the presence of OVs furnishes sites for the adsorption and activation of substrates. The overall concept suggests that augmenting a range of chemical properties within ABO_3 through the introduction of the OV state is likely to significantly enhance their established catalytic performance. This, in turn, could extend their applicability to previously unexplored domains, further expanding their potential applications.

3.2. Tuning band gap and electronic conductivity

The O 2p-band center's position relative to the Fermi level, as described by band theory, is a key descriptor of perovskite oxides' electrocatalytic activity. It reveals B–O hybridization and covalent bond properties, enabling swift assessment of catalytic performance through surface energy interactions. Fine-tuning the O 2p-band center to an optimal position enhances the engineered catalyst's electrochemical reaction capabilities.[68,147–150] Hong *et al.*[121] explored the band gap centers within a set of 10 perovskite oxides (Fig. 8a), analyzing how these centers influence both the M–O covalency and the electrocatalytic potential related to the oxygen evolution reaction (OER). Furthermore, as shown in (Fig. 8b), a clear correlation was found between the decrease in charge-transfer energy and the decrease in Fermi levels to the O 2p-band center in semi-metallic oxides. The closer congruence of the Fermi level with the O 2p band inside these compounds is

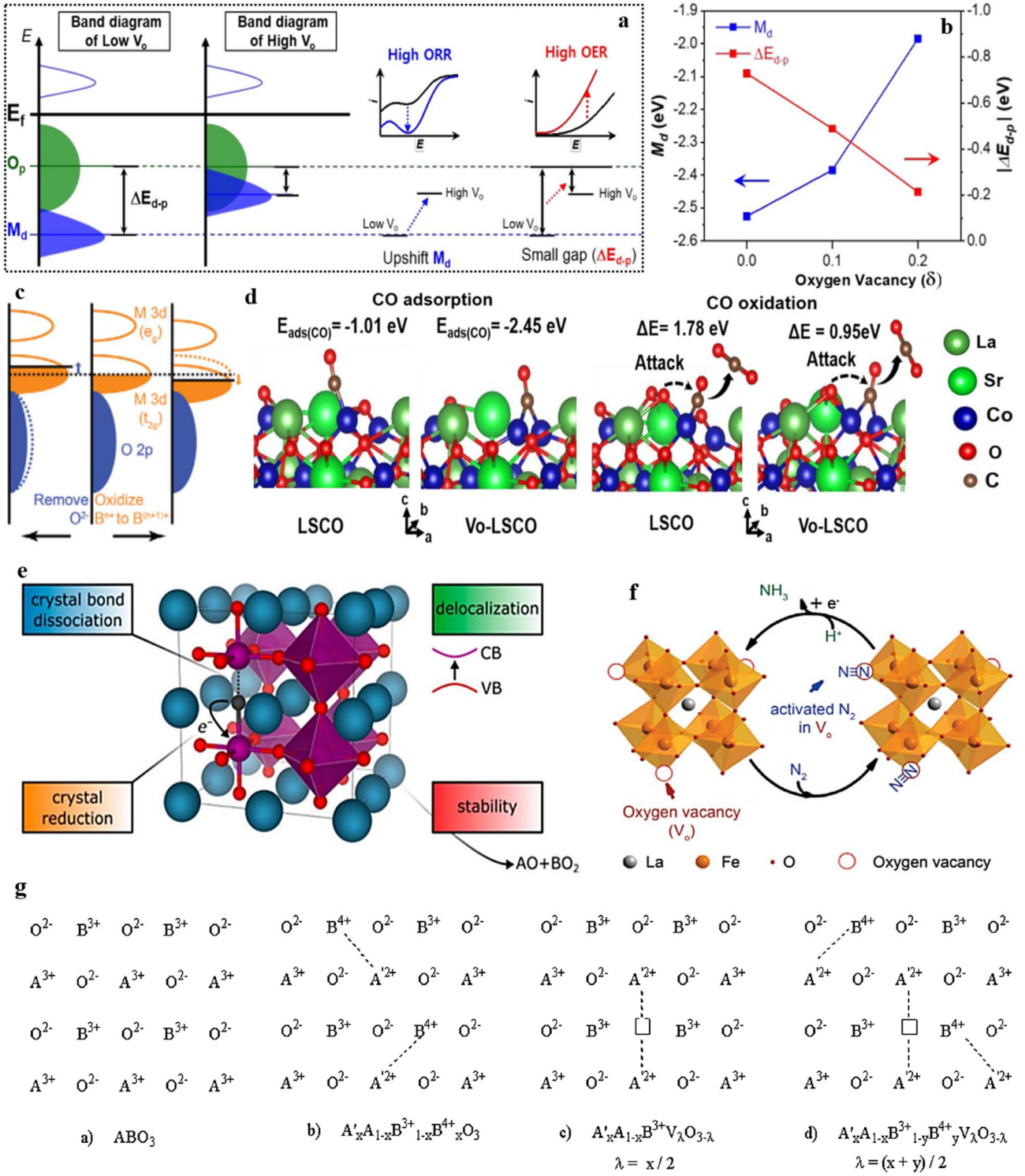

Fig. 7 (a) Rigid band illustrations of the late TMOs. (b) Deviation of the energy level alterations between Md and Op (ΔE_{d-p}) in the $Sm_{0.5}Sr_{0.5}CoO_{3-\delta}$ upon OVs induction. Reproduced from ref. 140 with permission from ACS, copyright 2020, (c) illustration of perovskite oxide bands organization following the O^{2-} exclusion and B^{n+} oxidation. Reproduced from ref. 107 with permission from RSC, copyright 2015, (d) configurations of CO with intended energy for the rate-determining step at OV sites on $La_{0.8}Sr_{0.2}CoO_3$ (LSCO). Reproduced from ref. 143 with permission from ACS, copyright 2019, (e) OV formation in ABO_3, reproduced from ref. 144 with permission from ACS, copyright 2021, (f) projected NO_3^- reduction mechanism on the OV-containing Cs, Ni-doped $LaFeO_{3-\delta}$. Reproduced from ref. 145 with permission from Elsevier, copyright 2019, (g). Alteration in the oxidation state (B-site cation) and the production of OV in the $A^{3+}_{1-x}A'^{2+}_xBO_3$ structure. Reproduced from ref. 146 with permission from Elsevier, copyright 1989.

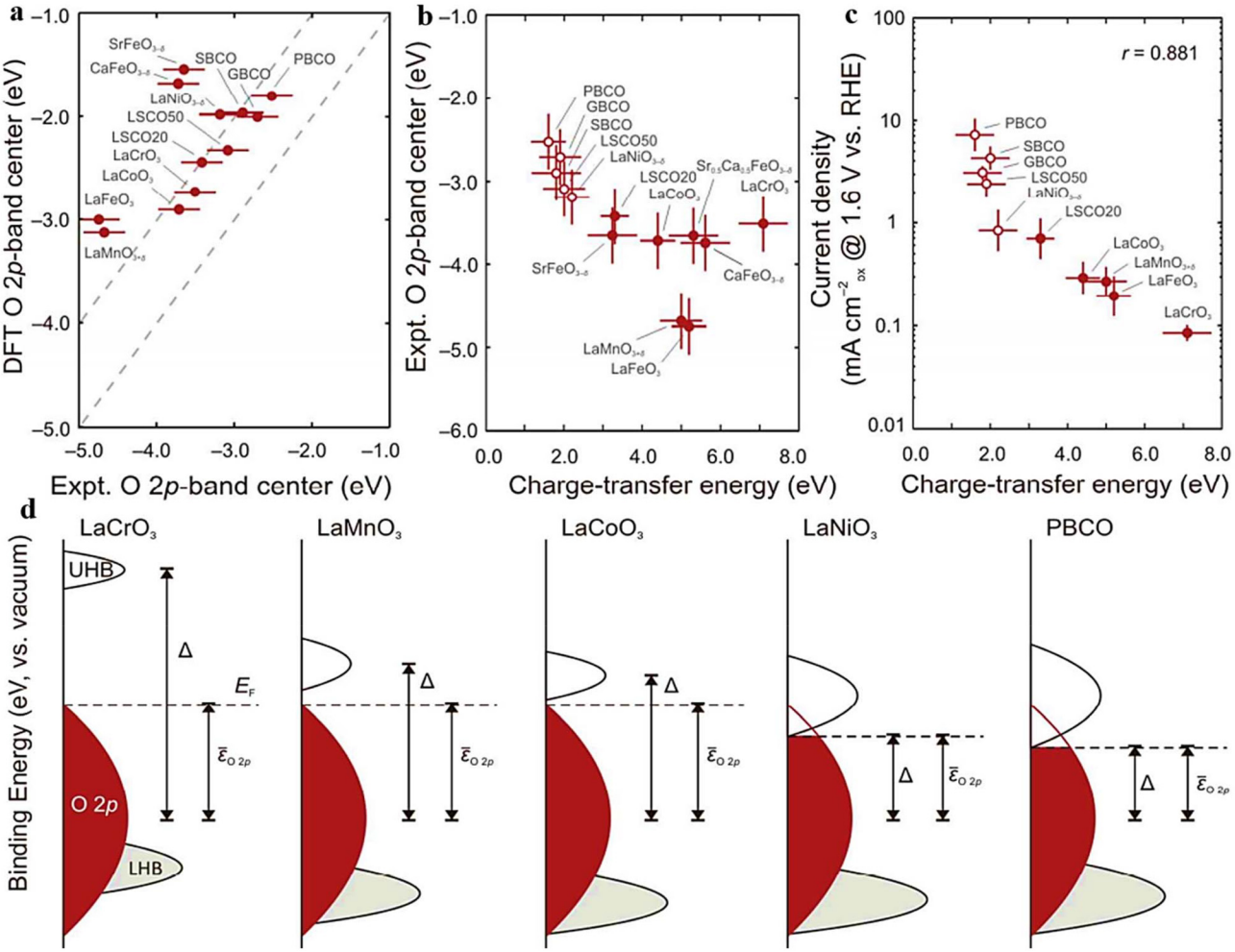

Fig. 8 (a) Comparative assessment of DFT and experimental O 2p bands relative to Fermi level. (b) The O 2p-band center's reliance on the charge-transfer energy (c) OER current *vs.* RHE at 1.6 V and charge-transfer energy (Δ) correlation (d) relationship between the positions of the Δ O, 2p (red) and M 3d (gray) bands. The M 3d band is segregated into the upper and lower Hubbard bands (UHB and LHB, respectively). Reproduced from ref. 121 with permission from ACS, copyright 2014.

induced by rising covalency, according to this connection. On the other hand, semiconducting oxides showed an irregularity. In this case, for p-type semiconductors, the charge-transfer energy did not affect the interaction between the Fermi level and the O 2p-band center.[121] It's important to highlight that the positioning of the O 2p-band center concerning the Fermi level is linked to the degree of metal–oxygen covalent bonding in semi-metallic oxides. However, this correlation between occupancy and covalency does not hold for semiconducting oxides that possess a band gap (Fig. 8d). In a similar vein, perovskite oxides with heightened electronic and ionic conductivity often exhibit enhanced electrocatalytic potential, as electrochemical reactions inherently involve electron migration. Incorporating multi-valent elements into the B-site and coupling them with A-site doping results in a multitude of perovskite materials showcasing a fusion of ionic and electronic conductivity.[151,152] Numerous techniques have been established for adjusting the electronic configuration (band centers) of perovskite oxides, aiming to boost their catalytic effectiveness. Among the various approaches explored, extensive research has been conducted on altering the constituents at the A and B-sites to fine-tune the electronic configuration within the synthesized catalyst material.[105,153,154]

3.2.1. Tuning B-site elements. The electronic configuration of cations occupying the B-site significantly influences their electrical conductivity. According to the findings of earlier studies, the transition-metal cation that is located at the B-site serves as a universal measure of activity in perovskite catalysis. This cation has a considerable impact on the mobility of oxygen ions, the availability of active sites, and the adsorption of water at the surface of perovskite oxides.[155,156] This leads to the manifestation of various traits in specific perovskite oxides, spanning from semi-conductive to potentially metallic conductive attributes. Hence, to create perovskite oxide catalysts with exceptional performance, it is logical to replace the B-site cations with alternative elements. The presence of OVs

and the overall electronic structure of the cations on the B-site may be affected by these substitutions in a particular perovskite oxide, thereby promoting the adsorption and release of reaction intermediates, ultimately facilitating effective catalysis. As an example, precise control over the Ni/Mn ratio resulted in the synthesis of a notably conductive substance denoted as $La_{0.5}Sr_{0.5}Mn_{0.9}Ni_{0.1}O_{3-d}$ (LSMN) as indicated in reference.[157] By leveraging its remarkable conductivity and harnessing the redox potential of transition metals, LSMN attains an increased quantity of active centers. These centers play an essential role in augmenting the electrocatalytic competencies of the engineered material. The redox pairs $Mn^{3+/4+}$ and $Ni^{2+/3+}$ establish reactive sites within LSMN through the adoption of both high spin (Mn^{3+} ($3d^4$)) and low spin (Ni^{3+} ($3d^7$)) configurations, facilitating orbital overlap that enhances electrochemical performance. The active sites on conductive catalysts are determined by double-phase boundaries (DPB), which are formed by the intersections of catalyst surfaces with the electrolyte, as shown in (Fig. 5b). In the present scenario, LSMN exhibits ample conductivity, resulting in the formation of continuous DPBs as the predominant reaction sites (Fig. 9b). Likewise, taking $NdBa_{0.75}Ca_{0.25}Co_2O_{5+\delta}$ (referred to as NBCC) as an exemplar of double perovskite oxides, researchers have unearthed that substituting B-site ions ($Co^{3+/}Co^{4+}$) with aliovalent analogs (Fe^{2+}, Ni^{2+}, or Mn^{2+}) gives rise to the development of $NdBa_{0.75}Ca_{0.25}Co_{1.5}M_{0.5}O_{5+\delta}$ (designated as NBCCM, where M = Fe, Ni, or Mn). This substitution not only triggers the creation of OVs (Fig. 9c and d) but also imparts heightened catalytic activity, as evidenced in (Fig. 9e). Furthermore, there was a prevailing taking that these OVs could establish interconnected pathways for oxygen species, including molecules like O_2, O_2^- ions, and OH^- ions. This arrangement facilitates a rapid OH^- exchange rate, thus contributing positively to the ORR.[158] Xu and his team[159] fabricated $SrFe_{0.9}Si_{0.1}O_{3-\delta}$ (SFSi) by integrating silicon into the B-site of an iron-based $SrFeO_{3-\delta}$ (SF) perovskite, uncovering the capability to systematically adjust the electroanalytic proficiency for the OER. Notably, a striking observation emerged as SFSi exhibited a lower-voltage than SF during the onset of the water oxidation current, signifying an enhanced OER activity resulting from the introduction of silicon (Fig. 9f). Furthermore, SFSi demonstrated a considerably reduced charge transfer resistance compared to SF, underscoring the silicon dopant's capacity to expedite charge transfer during the OER. This effect is probably linked to the elevated electrical conductivity of SFSi in contrast to SF (Fig. 9g). The increase in catalytic activity witnessed in SFSi can be attributed to the phase transition induced by Si-doping, which correlates with a decrease in Fe valency and a rise in the number of OVs (Fig. 9h). Duan and colleagues[160] examined the effect of iron on $LaCoO_3$ electronic structure to alter the Co 3d–O 2p covalent bonding to improve the Oxygen Evolution Reaction. Fe increases the overlap between Co (3d) and O (2p) states, reducing the energy difference between occupied and unoccupied states. Therefore, the Co 3d–O 2p covalent connection is reinforced (Fig. 9i–l). This increased covalency makes $LaCo_{0.9}Fe_{0.1}O_3$ a better OER catalyst than $LaCoO_3$.

3.2.2. Tuning A-site cation. In the standard arrangement of perfect perovskite oxides, it is widely accepted that the A-site cation does not directly participate in catalyzing the catalytic reaction. However, its impact can be perceived indirectly. For example, the introduction of substitutions at the A-site holds the capability to induce alterations in multiple attributes of perovskite oxides, including their electronic structure, the presence of OVs, and conductivity. Consequently, these changes contribute to the adjustment of the catalytic performance. In a recent research endeavor, Hwang and colleagues[150] investigated the influence of surface oxygen activity on the adsorption and surface coverage of NO_x, as well as the rate of NO oxidation, within the context of perovskite materials like $La_{1-x}Sr_xCoO_3$. Surface oxygen activity is defined as the positioning of the O 2p-band center relative to the Fermi level. The observation revealed that the introduction of Sr through substitution in $La_{1-x}Sr_xCoO_3$, up to a certain threshold (X = 0.2), enhances both the adsorption of NO_x and the efficiency of catalytic conversion within the given experimental conditions (Fig. 10a). The enhanced catalytic effectiveness was linked to the repositioning of the O 2p center closer to the Fermi level following the introduction of Sr substitution (Fig. 10b). The kinetics of NO oxidation displayed a distinctive pattern resembling a volcano, centered on $La_{0.8}Sr_{0.2}CoO_3$, and exhibited intrinsic activity comparable to state-of-the-art catalysts. The increased binding of NO (–NO–O_{oxide}) to oxygen sites resulting from elevated strontium substitution levels in $La_{1-x}Sr_xCoO_3$ brought about a notable decrease in the oxidation state of surface cobalt. This enhancement in surface cobalt reduction is connected to a decrease in the energy cost linked to the formation of surface oxygen vacancies (Fig. 10c). Likewise, in a recent investigation conducted by Sun and co-researchers,[161] a similar approach was taken to study the influence of introducing Li into the A-site of $CoCo_2O_4$. The study revealed that the gradual introduction of Li incorporation (($Co_{1-x}Li_x$) Co_2O_4 with x values of 0, 0.25, 0.5, 0.75, and 1) leads to a gradual elevation and closer alignment of the oxygen p-band center with the Fermi level (depicted in Fig. 10d). This alteration implies an enhanced reactivity of the oxygen ligands. As lithium cations replace the tetrahedral cobalt cations, the energy required for producing OVs consistently decreases (as depicted in Fig. 10e). Moreover, the authors conclude that the augmentation of lithium cations within the spinel structure of $(Co_{1-x}Li_x)Co_2O_4$ will lead to an improved capability for surface reconstruction, transitioning from a spinel to a layered configuration. It is evident that the incorporation of lithium brings about a noticeably enhanced catalytic effect, as evidenced by the nearly unaltered cyclic voltammetry (CV) curves of Co_3O_4, in contrast to the significant increase observed in $LiCo_2O_4$ after completing the cycling process (refer to Fig. 10f). A comparable trend of catalytic enhancement was observed in the case of A-site excessive modification in $(La_{0.8}Sr_{0.2})_{1+x}MnO_3$ (x = 0, 0.05, and 0.1) for the OER.[162] The catalytic effectiveness achieved through A-site modification was associated with the alignment of O 2p and M 3d energy centers closer to the Fermi level (Fig. 10g).

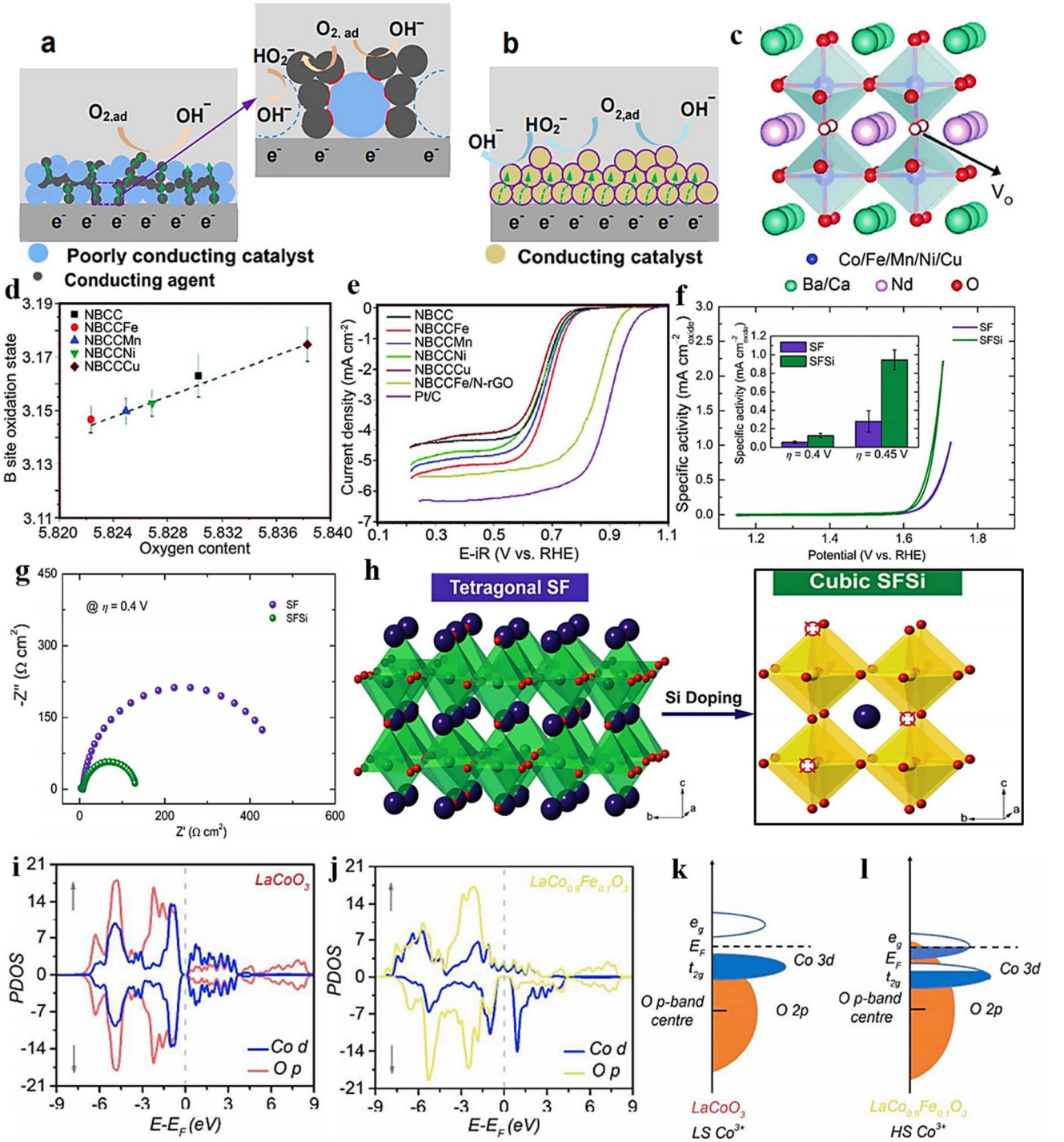

Fig. 9 Graphic illustrations of TPB and DPB. (a) Depicts the catalyst and electrolyte boundary. The inset highlights a discrete TPB interface (in red), delineated by poorly conducting catalysts, the electrolyte, and conducting agents. (b) The catalyst/electrolyte interface is in a single phase. The interface between intrinsically conductive catalysts and the electrolyte defines DPB (highlighted in violet color). Reproduced from ref. 157 with permission from ACS, copyright 2016, (c) crystal organization, (d) oxygen contents, and (e) linear sweep voltammograms of ORR catalysts (NBCC). Reproduced from ref. 158 with permission from RSC, copyright 2018, (f) the catalysts (SF and SFSi) were assessed for their OER activity using cyclic voltammetry (CV) scans in a 0.1 M KOH solution. The inset depicts the relationship between specific activity and overpotentials of η = 0.4 and 0.45 V. (g) EIS Nyquist plots of the catalysts (SF and SFSi) noted at an overpotential of η = 0.4 V. (h) Induced phase transition caused by Si-dopping. Reproduced from ref. 159 with permission from Wiley, copyright 2018, (i) pDOS of the Co d and O p states in $LaCoO_3$ (j) and $LaCo_{0.9}Fe_{0.1}O_3$. (k and l) Graphic depiction of overlap between Co 3d–O 2p for $LaCoO_3$ and $LaCo_{0.9}F_{e0.1}O_3$. Reproduced from ref. 160 with permission from ACS, copyright 2017.

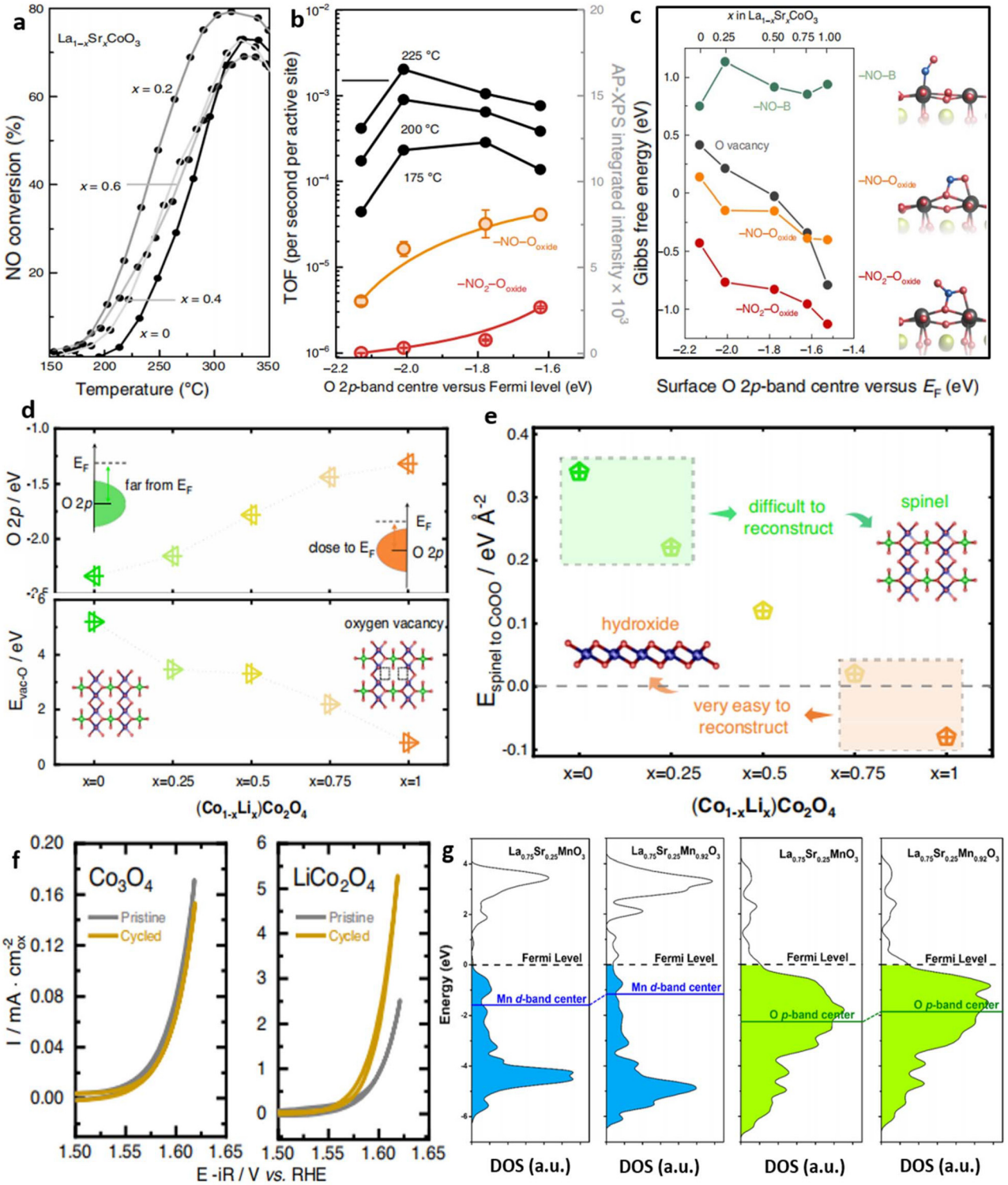

Fig. 10 Oxidation kinetics of NO investigated on powder $La_{1-x}Sr_xCoO_3$ (x = 0, 0.2, 0.4, and 0.6) under a NO: O_2 (g) inlet ratio of 1 : 200. (b), The TOF analysis for NO oxidation to NO_2 as a function of the O 2p-band center of the (001) surface relative to the Fermi level of $La_{1-x}Sr_xCoO_3$ at various temperatures. (c) Gibbs free energy of OV formation (OV, grey), and for the NO adsorption on the catalyst surface as a function of the surface O 2p-band center concerning the Fermi level, EF. The binding orientations of NO and NO_2 on cobalt (represented by grey spheres) and oxygen (represented by red spheres) are illustrated, with nitrogen depicted as blue spheres and lanthanum or strontium depicted as green spheres. Reproduced from ref. 150 with permission from Nature, copyright 2021, (d). Computed O p-band center OV creation energy (EO-vac) of spinel $(Co_{1-x}Li_x)Co_2O_4$ (x = 0, 0.25, 0.5, 0.75 and 1). (e). The energy changes from spinel to layered species on the surface. The cyclic voltammetry (CV) pattern of both pristine and cycled spinel Co_3O_4 and $LiCo_2O_4$. Reproduced from ref. 161 with permission from Nature, copyright 2023, (g). Diagrams of PDOS for Mn d-band and Mn d-band center comparative to the Fermi surface of $La_{0.75}Sr_{0.25}MnO_3$ and $La_{0.75}Sr_{0.25}Mn_{0.92}O_3$ are presented, along with the O p-band and O p-band centers relative to the Fermi surface of the same materials. Reproduced from ref. 162 with permission from ACS, copyright 2019.

4. Strain engineering

Recently, the utilization of strain engineering in nanostructures has attracted considerable interest and has proven to be a powerful method for tailoring the surface electronic arrangement, altering the bonding between metals and oxygen, and influencing the catalytic properties of nanomaterials (Fig. 11a).[142] As a result, this technique holds substantial importance both in principle and in practical terms for a diverse array of applications.[142,163,164] Strain (measured in dimensionless units) refers to the distortion experienced by a solid due to stress (measured in units of Pascals). Stress is defined as the external force exerted on a specific area. Generally, tensile strain is advantageous for enhancing performance, while compressive strain should be minimized in electrochemical processes.[165–168] Nevertheless, recent studies have highlighted the significance of compressive strain in enhancing catalytic reactions.[169,170] As an illustration, when compared to films that are unstressed and in a relaxed state, the $LaNiO_3$ film subjected to compressive strain exhibited remarkable bifunctional capabilities that outperformed even catalysts based on noble metals (Fig. 11b and c).[171] This remarkable achievement was linked to the effect of compressive strain, which influenced the occupation of dz 2 (out-of-plane) orbitals and led to an uneven distribution of e_g-derived orbitals within the BO_6 octahedron (Fig. 11d). Aside from alterations in structure, strain can also alter the energies associated with the formation and movement of oxygen defects.[172,173] Notably, the energy required to form an oxygen vacancy in perovskite can be significantly decreased, resulting

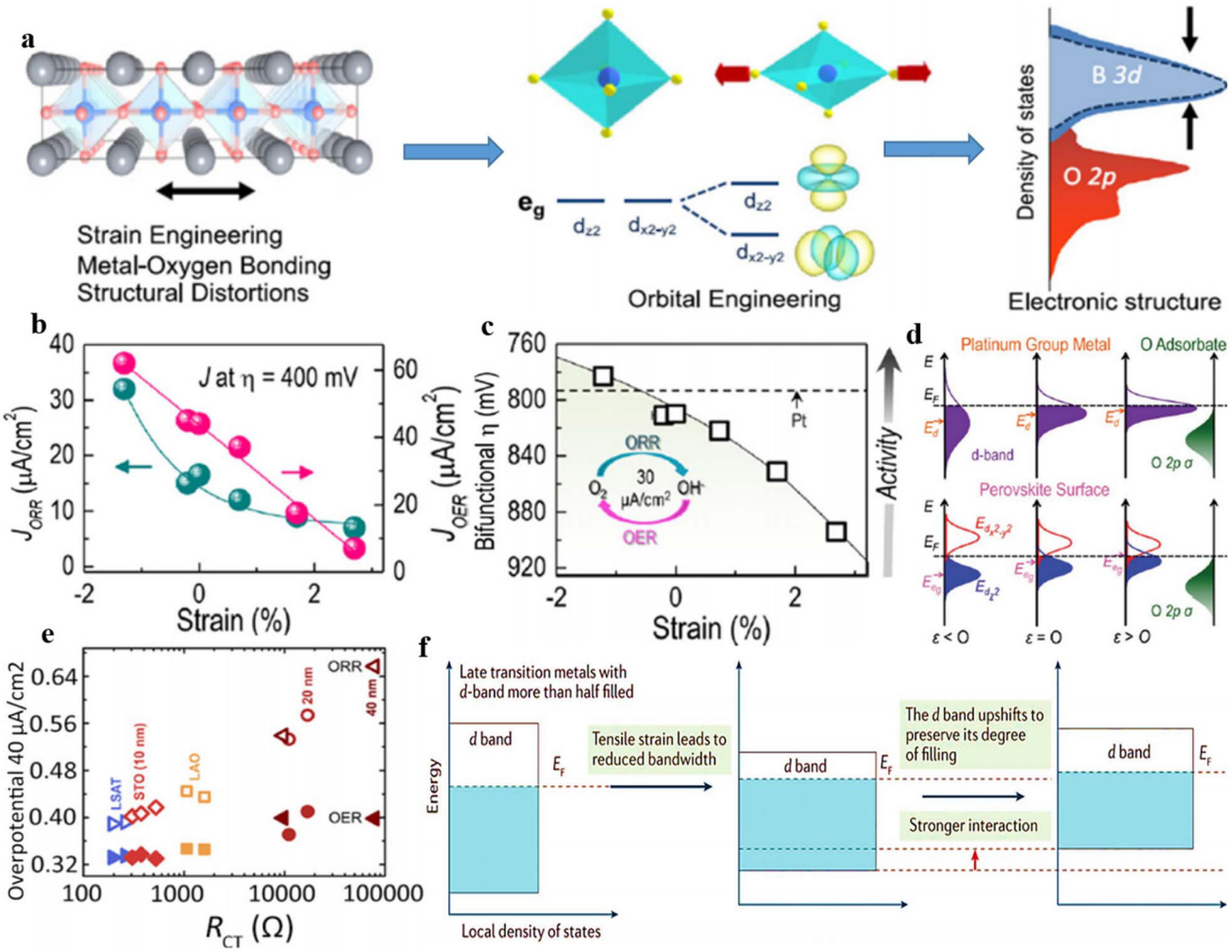

Fig. 11 (a) Strain-induced structural changes lead to the splitting of formerly degenerate orbitals, resulting from symmetry disruption. Meanwhile, changes in M–O orbital overlap impact the widening of d-states. Reproduced from ref. 142 with permission from Elsevier, copyright 2019, (b) current densities (J) of the corresponding OER and ORR at overpotentials of g = 400 mV. (c) Compressed $LaNiO_3$ surpasses Pt and IrO_2 to achieve 30 lA cm^{-2} for both reactions, demonstrating its superior bifunctional capability, (d) the trend in perovskites, depicted in schematics, correlates with the d-band center (E_d) in Pt. While changes in bandwidth significantly influence E_d shifts for Pt group metals, correlated oxides like LNO are more affected by orbital splitting and polarization on their asymmetric surfaces. Reproduced from ref. 171 with permission from ACS, copyright 2016. (e) The relationship between charge transfer resistance and overpotential. Reproduced from ref. 165 with permission from ACS, copyright 2015, (f) illustration of the effect of tensile strain on the d-band center. Reproduced from ref. 177 with permission from Nature, copyright 2017.

in a notable increase in OV concentration and consequently leading to enhanced performances.[174] Moreover, strain can also impact the kinetics of charge transfer occurring at the surface of the catalyst.[175] For instance, among the various materials examined, the LCO ($LaCoO_3$) thin films grown on an LSAT [$(LaAlO_3)0.3(Sr_2AlTaO_6)0.7$] substrate demonstrated the most eminent catalytic performances in an alkaline environment (Fig. 11e).[176] This result can be credited to the existence of a moderately tensile strain brought about by the substrate and film thickness. The enhancement originated from the decrease in resistance to charge transfer on the surface of LCO. Density Functional Theory (DFT) has additionally been employed to investigate the underlying causes of how surface strain influences binding energies. This analysis involved compiling data from diverse systems subjected to both strained and unstrained conditions. The diagram depicted in (Fig. 11f) illustrates the displacement of the d-band center for late transition metals (with a d-band that's more than half-filled) when subjected to tensile strain.[177] The displacement of the d-band center is a result of modifications in the quantity of adjacent metal atoms; a decrease in coordination results in a narrower local bandwidth and an elevated d-band center. It is evident that applying tensile strain reduces coordination numbers, ultimately leading to a narrowing of bandwidth and an upward shift of the d-band center. The importance of the d-band center stems from its involvement in the interplay between adsorbate states and metal d states, a critical factor in determining the energy of interaction.

5. Application of perovskite oxides in NO_3^- reduction

The perovskite oxide family has been identified as a highly promising class of catalysts, distinguished by their exceptional activity, structural flexibility, and compositional tunability. The synergistic interplay between the intrinsic activity of metal site and OVs underlies their enhanced catalytic performance in electrochemical conversion reactions, highlighting the critical importance of OVs in the rational design of optimized perovskite-based catalysts[61,65,178] The exceptional characteristics of perovskite oxides have stimulated significant research attention towards their utilization as a novel class of materials for the electrochemical conversion of NO_3^- pollutants into NH_3, a highly valued product, thereby showcasing their potential in waste-to-wealth technologies. The unique characteristics of perovskite oxide-based electrocatalysts have recently been recently reported in terms of current density, efficiency, and conversion rate in (Table 1).

For example, Zhang *et al.*[118] investigate the catalytic capabilities of perovskite oxides in converting NO_3^- to NH_3, with a particular focus on understanding the influence of OVs. In their experimental approach, they synthesized four distinct perovskite oxides (A = La; B = Cr, Mn, Fe, Co) with varying crystal structures and OVs. Based on XPS and EPR studies, the analysis of OVs revealed that among the other perovskites, $LaCoO_3$ with a hexagonal structure exhibited the highest concentration of OVs. The O 1s XPS spectra displayed an OV peak at 531.4 eV for the synthesized materials, with $LaCoO_3$ accounting for 47.1% in comparison to $LaFeO_3$ (41.5%), $LaMnO_3$ (33.5%), and $LaCrO_3$ (27.6%) (Fig. 12a). These results demonstrate that $LaCoO_3$ possessed the highest amount of OVs among the investigated perovskites. Likewise, the EPR signal intensity at around 2.02 g was significantly higher for $LaCoO_3$ compared to the other perovskites examined, providing further evidence of an elevated quantity of OVs in this particular material (Fig. 12b). The investigation of electrochemical performance revealed that the $LaCoO_3$ electrode outperforms the $LaMnO_3$, $LaCrO_3$, and $LaFeO_3$ electrodes in terms of NO_3^- reduction to NH_3 Notably, the $LaCoO_3$ electrode demonstrates a significantly higher faradaic efficiency of 91.5% and a greater NH_3 yield rate of 4.18 mmol mg^{-1} h^{-1} at −1.0 V (*vs.* RHE) when compared to the other perovskites (Fig. 12c and d). The current density profile indicates that among the other materials, $LaCoO_3$ displayed the highest value of 346 mA cm^{-2} at −1.5 V when compared to a value of 184 mA cm^{-2} in the absence of NO_3^- ions, confirming the electrochemical conversion of NO_3^- into NH_3 (Fig. 12e and f). In combination with the electrochemical findings, XPS, and EPR investigation, the improved performance of $LaCoO_3$ in NO_3^- reduction to NH_3 can be attributed to its elevated level of OVs, which are induced by abundant lattice distortions in its hexagonal structures. Moreover, an examination of the material's structure, OVs, and oxidation states of the metal in $LaCoO_3$ remained

Table 1 The summary of the performance (including current density, efficiency, and conversion rate) of perovskite oxides in the conversion of NO_3^- to NH_3

Catalyst	Current density	Conversion rate	Efficiency	Ref.
$LaSrNiCoMnFeCuO_3$ PNTs	−0.9 V_{RHE}	1657.5 μg h^{-1} $mg_{cat.}^{-1}$	100%	179
FeCo alloy	−0.9 V_{RHE}	17.2 mg h^{-1} mg_{cat}^{-1}	90.3%	180
$(Ba_{0.5}Sr_{0.5})_{1-x}Co_{0.8}Fe_{0.2}O_{3-\delta}$	−0.45 V_{RHE}	143.3 mg h^{-1} mg_{cat}^{-1}	97.9%	181
$NbWO_{6-x}$	−0.7 V_{RHE}	0.068 mmol h^{-1} mg cat^{-1}	85.7%	182
La_2CuO_4	−1.0 V_{SCE}	—	29.3%	183
RS-$BiFeO_3$	−0.7 V_{RHE}	5.3 mg cm^{-2} h^{-1}	86.8%	184
$LaCoO_3$	−1.8 V_{RHE}	—	85%	185
$LaFe_{0.9}Ru_{0.1}O_3$	−0.8 V_{RHE}	0.75 mmol h^{-1} cm^{-2}	98.5%	186
$LaCoO_3$	−1.0 V_{RHE}	4.18 mmol mg^{-1} h^{-1}	91.5%	118
Mn-incorporated Co_3O_4 nanotubes	−1.2 V_{RHE}	35 mg h^{-1} cm^{-1}	99.5%	187

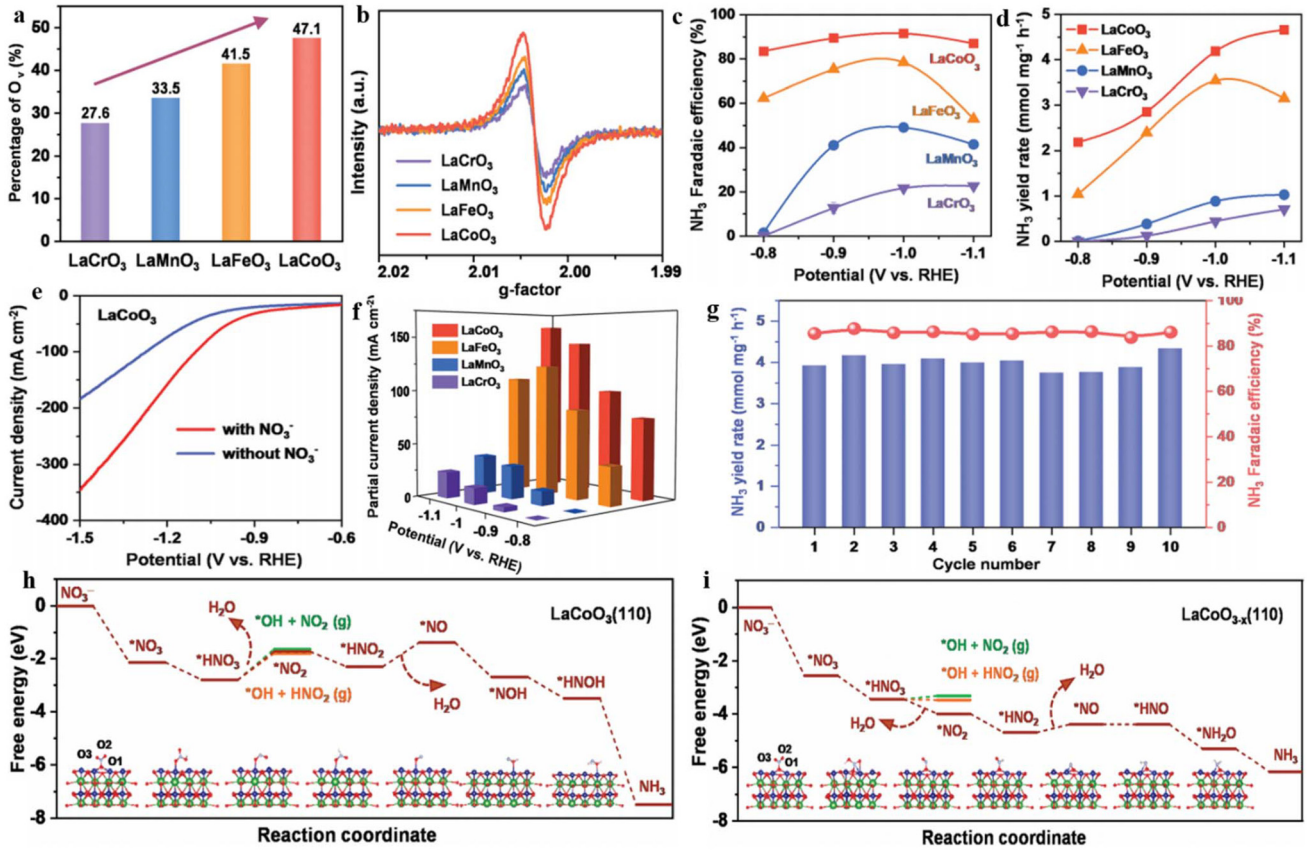

Fig. 12 (a) The percentage of OVs for applied materials from the XPS examination. (b) EPR spectra of different catalysts used. (c and d) The assessment of FE and NH_3 yield rate. (e and f) LSV investigation for $LaCoO_3$ electrode in the presence and absence of NO_3^-, respectively, and partial current density at different potentials. (g) NH_3 yield rate and respective FE throughout the successive recycling assessment of $LaCoO_3$ electrode at −1.0 V (*vs.* RHE). (h and i) Free energy diagrams for NO_3^- catalysis resulting in NH_3 production on (h) $LaCoO_3$(110) in absence of OVs and (i) $LaCoO_{3-x}$(110) presence of OVs. Reproduced from ref. 118 with permission from Wiley, copyright 2023.

unaltered after catalysis, signifying its stability for repeated cycles. By conducting DFT analysis, it was revealed that the existence of oxygen vacancies in $LaCoO_3$ provides stability to intermediate species, reduces the energy barrier for conversion of NO_3^- to NH_3, and impedes the formation of undesired by-products (NO_2 and HNO_2). When comparing the NO_3^- binding mechanism of $LaCoO_3$ without OVs to the $LaCoO_{3-x}$ (110) structure, notable differences were observed. In the absence of OVs, O1 of NO_3^- binds to the surface CO atom while O_2 and O_3 remain exposed. Conversely, in the presence of OVs, O1 of NO_3^- binds to the OV site, while O2 binds to the CO atom exposed on the $LaCoO_{3-x}$(110) structure (Fig. 12h and i). This observation suggests that the OVs in the prepared material provide an additional binding site that helps stabilize the NO_3^- ions. These critical factors significantly contribute to the exceptional catalytic activity and selectivity observed in the synthesized $LaCoO_3$ perovskite, which is enriched with OVs.

Despite cobalt-based perovskite oxides showing significant promise in electrocatalysis,[188,189] their potential for enhancing eNO_3RR in NH_3 production has remained unexplored until now. To address this research gap, Liu *et al.*[190] have presented a solution to this research gap by introducing an effective strategy that involves manipulating A-site deficiencies in cobalt-based perovskite oxides. This approach aims to tune the physicochemical properties, such as OVs and band center, to enhance the conversion capability of NO_3^- to NH_3. In their study, they examined a series of catalysts, specifically $(Ba_{0.5}Sr_{0.5})_{1-x}Co_{0.8}Fe_{0.2}O_{3-\delta}$, with varying x values of 0, 0.05, 0.10, 0.15, and 0.20, to showcase their approach. The introduction of deficiencies in the prepared material was examined through an XRD study, which revealed that the position of the main peak associated with the (110) plane exhibited a slight shift towards higher angles as the A-site cation deficiencies increased (Fig. 13a). XPS analysis indicates that the percentage of OVs in the prepared samples increased with increasing x value (Fig. 13b), while the valence states at the B site remained unaffected (Fig. 13d). Approximately 38.0%, 39.9%, 49.6%, 53.4%, and 55.1% of OVs were found in (BS)0.95CF, (BS)0.90CF, (BS)0.85CF, and (BS)0.80CF, respectively (Fig. 13c).

During the assessment of their catalytic performance in NO_3^- electro reduction for NH_3 synthesis, the findings indicated a peak at x = 0.15, coinciding with (BS)0.85CF catalyst. This specific catalyst demonstrated remarkable selectivity (97.9%) and impressive stability (200 h), thereby emphasizing its excellent performance in

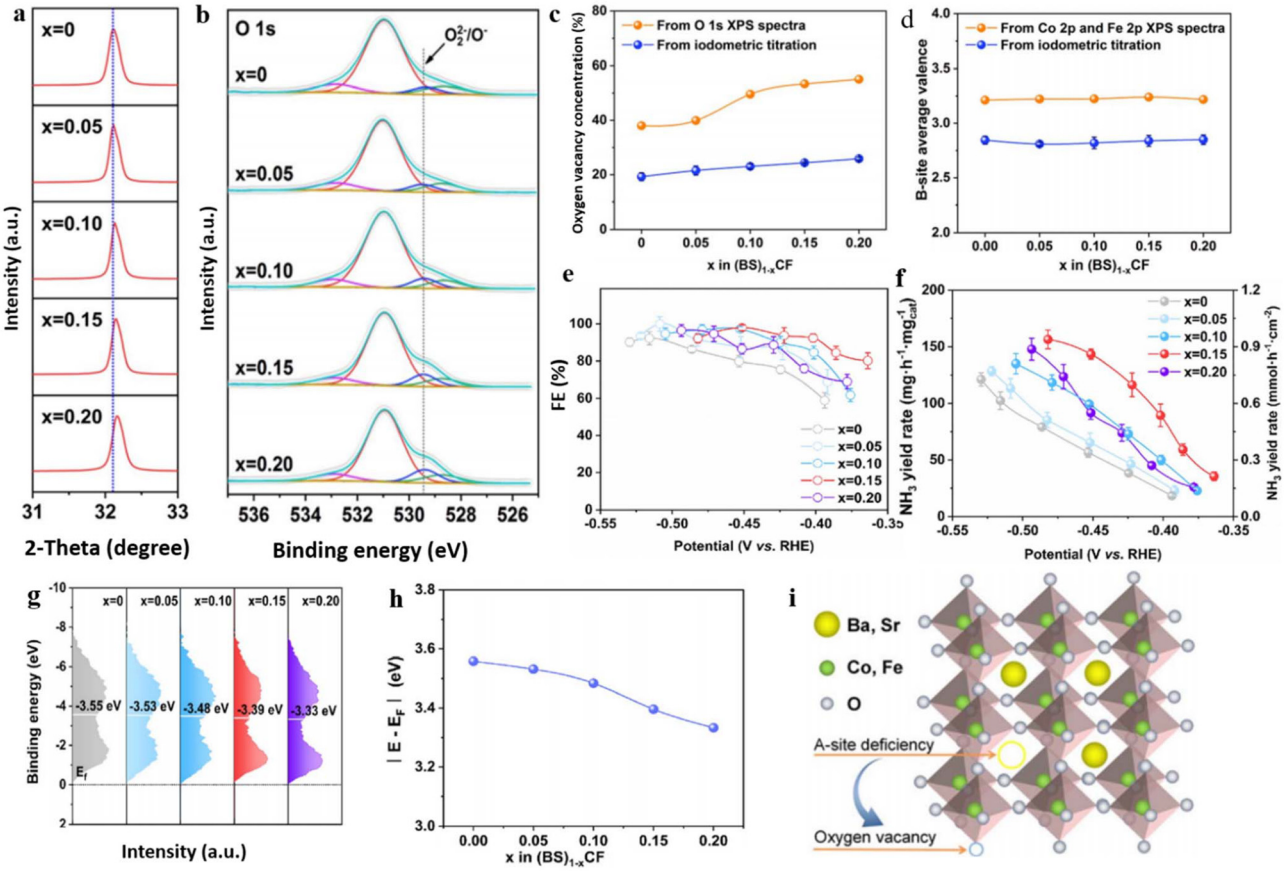

Fig. 13 (a) XRD data (Rietveld refinement plots) of the $(BS)_{1-x}CF$ samples ($2-\theta$ of 31–33°). (b and c) O 1s XPS spectra. (d) Amount of OVs, and (e) average valence states of B-site acquired from XPS and iodometric titration analyses, respectively. (e and f) FE and yield rate at multiple potentials. (g and h) XPS spectra of surface valence band, and the band center calculated from surface valence band XPS spectra for the $(BS)_{1-x}CF$ catalysts. (i) Graphic photograph of the induction of OVs in A-site-deficient $(BS)_{1-x}CF$. Reproduced from ref. 190 with permission from RSC, copyright 2023.

ammonia synthesis (0.86 mmol h^{-1} cm^{-2}) (Fig. 13e and f). The excellent performance of (BS)0.85CF, surpassing the others, can be ascribed to the presence of a moderate quantity of OVs. Excessive OVs have the potential to impede the formation of electron holes and redox couples, and in extreme cases, they can cause structural collapse.[191,192] Furthermore, this manipulation induces a gradual shift of the band center towards the Fermi level as the x values increase. The calculated values from the Fermi level exhibited the following order: (BS)0.95CF (3.55 eV) > (BS)0.90CF (3.48 eV) > (BS) 0.85CF (3.39 eV) > (BS)0.80CF (3.33 eV) (Fig. 13g and h). These values demonstrated a proportional decrease with the increase in A-site deficiencies or the presence of OVs. The authors proposed that the enhanced electrochemical performance can be primarily attributed to the stronger affinity between the oxygen atom of NO_3^- and the OV sites and modulation of Fermi level distance in the designed catalyst. The stronger affinity facilitates the adsorption of NO_3^- and enables its subsequent reduction to NH_3 with high selectivity, while simultaneously impeding the formation of unwanted by-products.[193]

OVs have found extensive application in enhancing the effectiveness of selective NH_3 synthesis through the utilization of catalysts based on tungsten (W). Notably, the incorporation of OVs in WO_{3-x} nanowires and nanosheets has demonstrated the ability to influence the adsorption of N species and partially suppress the competing HER.[194] As a result, it is plausible to expect that the presence of OVs in catalysts based on tungsten can significantly enhance the capture and reduction of N species. In recent times, there has been considerable interest in the utilization of W-based perovskite oxide that possesses the ability to manipulate OVs, primarily due to their high surface area, ultrathin thickness, and diverse composition of metallic oxides.[74] These characteristics make them highly promising for NH_3 synthesis. However, research focusing on nanosheets of W-based perovskite oxide with OVs for NO_3^- to NH_3 synthesis (NRA) remains limited. In this context, Feng *et al.*[182] conducted a study where they synthesized $NbWO_6$ perovskite oxide with incorporated OVs and evaluated its effectiveness as an electrocatalyst for the reduction of NO_3^- to NH_3. The results showed that the $NbWO_6$ nanosheets with OVs ($NbWO_{6-x}$) exhibited exceptional performance in terms of NH_3 selectivity and faradaic efficiency. The existence of oxygen vacancies (OVs) in the synthesized material was confirmed through several analytical techniques, including XPS, EPR, and Raman investigations. The O 1s XPS spectra displayed a dis-

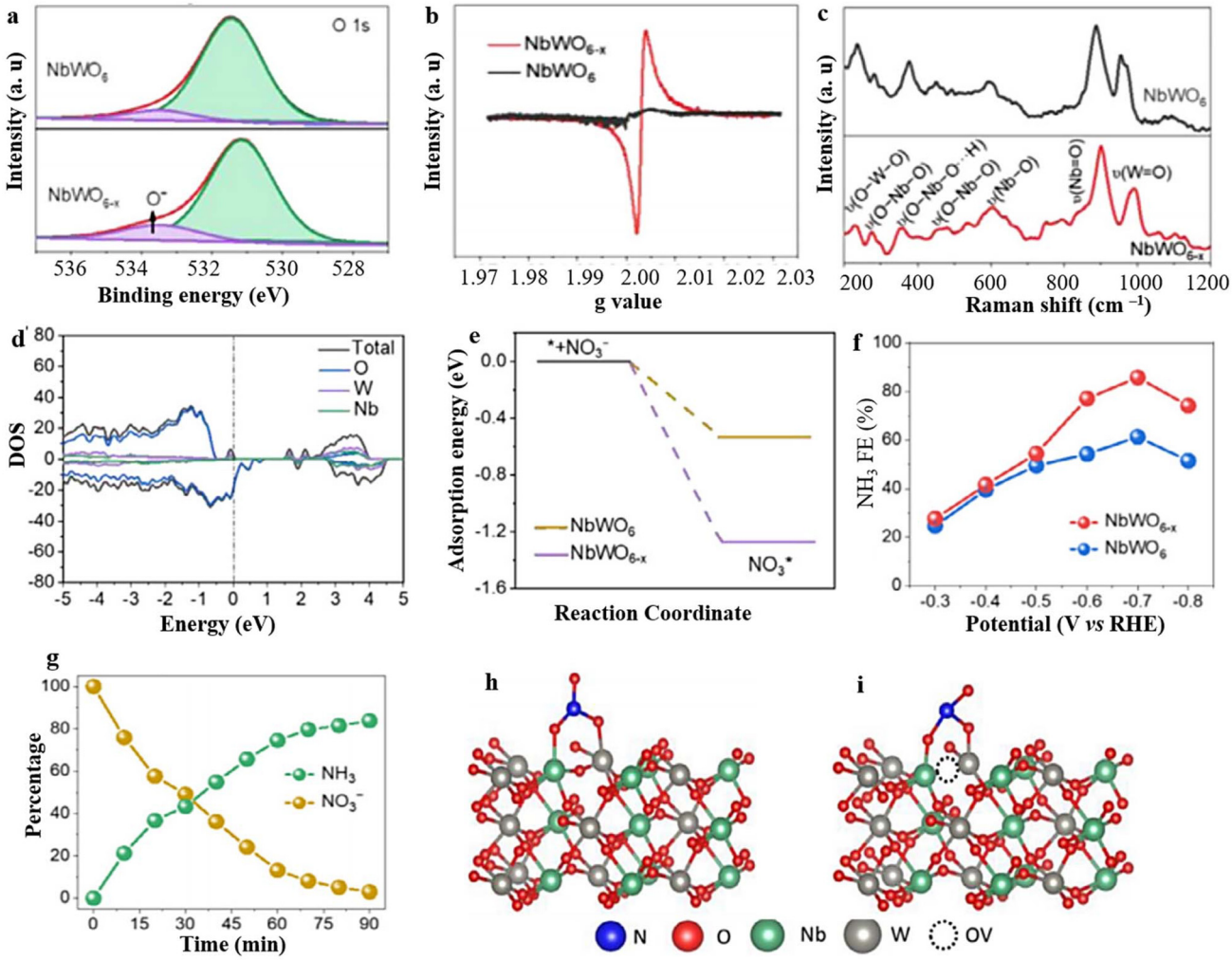

Fig. 14 (a) O 1s XPS, (b) EPR, and (c) Raman spectra of $NbWO_6$ and $NbWO_{6-x}$. (d and e) The DOS and adsorption energies of NO_3^-. (f and g) FE (NH_3) and respective alteration in concetration of NO_3^- and NH_3 at different intervals, and (h and i) NO_3^- adsorption simulations of $NbWO_6$ and $NbWO_{6-x}$ respectively. Reproduced from ref. 182 with permission from Elsevier, copyright 2023.

tinct peak at 533.5 eV, while the EPR pattern exhibited a prominent signal at 2.004 g, providing conclusive evidence for the presence of OVs in the prepared material (Fig. 14a and b). Moreover, the Raman peaks of $NbWO_{6-x}$ nanosheets exhibited a broadening effect and shifted towards higher wavenumbers, further supporting the presence of OVs in $NbWO_{6-x}$ and providing additional insights into their characteristics (Fig. 14c). The density of states (DOS) analysis confirms the presence of defect energy levels in the conduction band of $NbWO_{6-x}$, which facilitates more efficient electron transitions. The induction of OVs on the $NbWO_{6-x}$ surface causes the Fermi level to shift near the conduction band minimum (Fig. 14d). This shift occurs due to the occupation of excess 4d electrons from tungsten (W). Consequently, $NbWO_{6-x}$ exhibits metallic behavior and improved conductivity, which is advantageous for electrochemical reduction processes. Additionally, the adsorption energy of NO_3^- on $NbWO_{6-x}$ (−1.27 eV) is significantly lower than that on $NbWO_6$ (−0.53 eV), promoting a higher affinity for NO_3^- adsorption (Fig. 14e). This enhanced adsorption capability further facilitates the conversion of NO_3^- to NH_3, as illustrated in (Fig. 14g). The mechanism was confirmed to involve tungsten (W) cations interacting with neighboring OVs and the specific d orbital electrons of $NbWO_{6-x}$. These interactions create unsaturated active centers that enhance the adsorption and activation of NO_3^-. This strengthened capability for NO_3^- adsorption contributes to a more favorable environment for NO_3^- reduction to NH_3 to occur (Fig. 14h and i).

Yin *et al.*[195] developed a perovskite oxide, $LaFeO_3$, that was modified with Cu, Mn, and Co at the B-site. The primary objective of this synthesis was to produce an electrocatalyst capable of facilitating the transformation of NO_3^- into NH_3. Among the various catalysts tested, Cu-doped $LaFeO_3$ exhibited the highest level of activity. At a potential of −1.1 V (*vs.* RHE), it achieved a significant NH_3 yield of 1005.0 μg h^{-1} cm^{-2}, while at −1.0 V (*vs.* RHE), it demonstrated an FE of 71.9%. This excellent electrocatalytic performance can be primarily attribu-

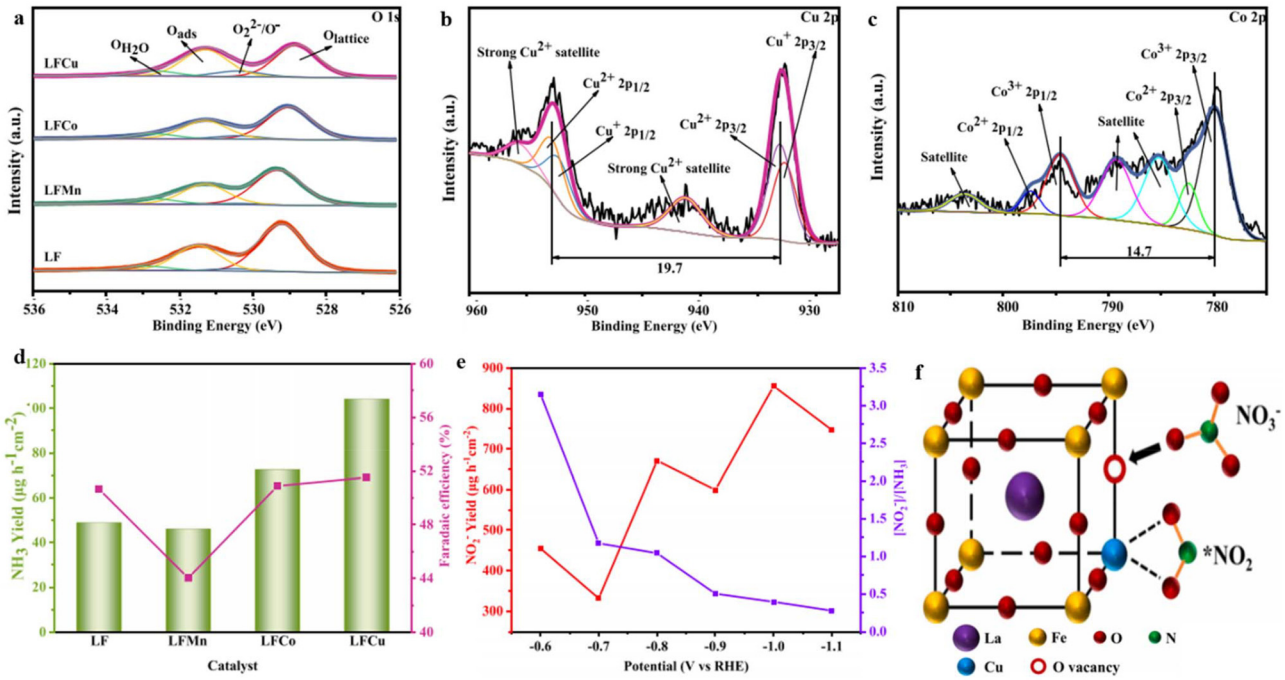

Fig. 15 (a–c) XPS spectra of O 1 s, Cu 2p of LFCu, and Co 2p of LFCo. (d) Yield rate and Fes (NH_3) of the respective catalysts at −0.7 V (*vs.* RHE). (e) NO_2^- production and the ratio of [NO_2^-] to [NH_3] on LFCu at various potentials, (f) schematic representation of NO_3^- reduction on LFCu. Reproduced from ref. 195 with permission from Elsevier, copyright 2023.

ted to the increased presence of OVs on the catalyst's surface resulting from the incorporation of copper. The XPS analysis of the O 1s spectra provided evidence of a relatively higher concentration of OVs in Cu-doped $LaFeO_3$ compared to other dopants (Fig. 15a). The incorporation of copper (Cu) in the catalyst proved more advantageous due to the presence of Cu^+/Cu^{2+} oxidation states, whereas cobalt (Co) existed as Co^{2+}/Co^{3+} (Fig. 15b and c). This disparity in charge between Cu and the substituted Fe^{3+} was more substantial, compared to the Co^{2+}/Co^{3+} states. Consequently, the investigation affirmed the positive impact of OVs on the catalyst's surface on the efficiency of NO_3^- reduction, as established in previous studies.[129,196] The presence of OVs in the catalyst facilitated the adsorption of NO_3^- by occupying the oxygen atoms within the vacancies, thereby weakening the N–O bonds. Additionally, the OVs, along with the Cu sites, readily interacted with the reaction intermediates, thereby enhancing the catalyst's conductivity. Furthermore, the catalyst exhibited remarkable stability and even displayed improved activity upon recycling, which can be attributed to the ferroelectric properties inherent in the catalyst. The selectivity of the catalyst during the electrochemical reduction of NO_3^- to NH_3 varied based on the applied potential. Lower applied potentials effectively minimized the generation of NO_2 as a byproduct (Fig. 15e).

Although many groundbreaking studies have focused on electrocatalyst development, a comprehensive grasp of the correlation between material characteristics and NO_3RR activity remains elusive. To explore this correlation, Gong *et al.*[197] conducted a study in which they synthesized various La_2CuO_4 perovskite materials by doping the B-site with Ni, Co, and Zn. The authors then inspected the influence of these dopants on the behavior of NO_3^- reduction. Among the materials synthesized, the perovskites based on Cu and Co exhibited significantly enhanced activity in the NO_3RR and demonstrated improved selectivity towards NH_3 synthesis. The analytical investigation revealed that the doping of the B-site effectively controlled the hybridization between the metal and oxygen, thereby resulting in finely tuned surface adsorption properties and improved NO_3RR activity. The O–K edge XAS analysis was conducted to examine the level of metal–oxygen hybridization. The gathered data revealed significant electronic excitation from the O 1s to O 2p–M 3d (530 eV), O 2p-La 5d (535 eV), and O 2p–M 4sp (543 eV) states[112] (Fig. 16a). Remarkably, Co and Ni doping resulted in heightened peak intensity, indicating a more pronounced metal–oxygen hybridization in these doped materials.[112,198] The crucial influence of M–oxygen hybridization on the catalytic activity of transition metal oxide/hydroxides has long been recognized, and the results of this study are similar to previous findings.[199,200] Moreover, there is a notable association between the current of NO_3^- reduction and the hybridization of M–oxygen. The $La_2Cu_{0.8}Co_{0.2}O_4$, characterized by the highest M–oxygen hybridization, displayed the greatest NO_3^- reduction current, potentially attributed to a more advantageous NO_3^- adsorption (Fig. 16b and c). It was observed that oxides with greater M–oxygen hybridization displayed increased nitrate coverage on surface sites, which was attributed to improved oxygen activity.[150,201,202] Consequently, the authors of this study found a significant correlation between

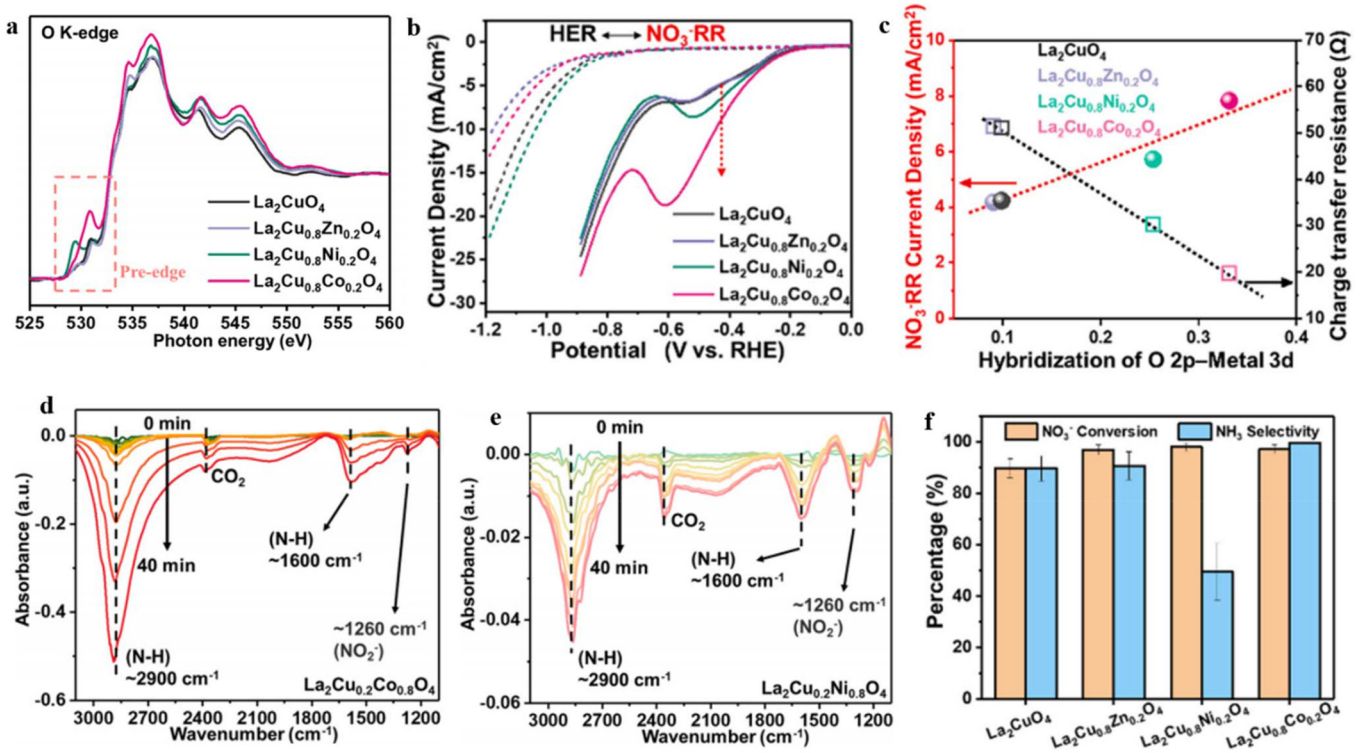

Fig. 16 O K-edge XAS spectra of the specified materials. (b) LSV curves for the La_2CuO_4, $La_2Cu_{0.8}Co_{0.2}O_4$, $La_2Cu_{0.8}Ni_{0.2}O_4$ and $La_2Cu_{0.8}Zn_{0.2}O_4$. In 0.5 M Na_2SO_4 solution in absence or presence of 2000 ppm nitrate. (c) Relationship of current density (NO_3^- reduction) *vs.* RHE, charge transfer resistance, and the O 2p-metal hybridization from the O K-edge XAS spectra. (d and e) *In situ* FT-IR analysis at −0.68 V *vs.* RHE for $La_2Cu_{0.8}Co_{0.2}O_4$ and $La_2Cu_{0.8}Ni_{0.2}O_4$, respectively. (f) NH_3 selectivity and NO_3^- conversion. Reproduced with ref. 197 with permission from Elsevier, copyright 2022.

M–oxygen hybridization and the current of nitrate electrolysis, suggesting that the improved adsorption of reaction intermediates during the NO_3^- reduction reaction contributed to this phenomenon. The infrared (IR) analysis further validated that Co doping exhibits higher effectiveness in accumulating the intermediate and facilitating its subsequent reduction to NH_3, in comparison to Ni doping (Fig. 16d and e). This was evident from the intensity of bands observed at approximately 1260 cm^{-1} (corresponding to the nitrite peak) and around 2900 cm^{-1} and 1600 cm^{-1} (associated with the NH_3 peak). By conducting a comprehensive analysis of all experimental findings, it was deduced that the superior nitrate reduction activity of $La_2Cu_{0.8}Co_{0.2}O_4$, resulting in the production of NH_3, can be attributed to its pronounced M-oxide hybridization (Fig. 16f). This characteristic facilitates the adsorption of reaction intermediates during the NO_3RR process while concurrently suppressing the activity of the HER on the surface.

Due to its exceptional adsorption capacity, biochar has gained significant popularity as a sorbent for environmental remediation. In recent times, several research investigations have concentrated on examining the photocatalytic efficacy of metal-modified biochar for eliminating water contaminants with high concentrations.[203–205] This material holds the potential to function as a rechargeable reservoir of bioavailable electrons, making it suitable for deployment as a photocatalyst in reduction reactions. However, the application of biochar composites with perovskite oxides as a photocatalyst for the efficient conversion of the NO_3^- pollutant into valuable NH_3 has not been investigated extensively. In their research, Liu *et al.*[206] synthesized composites of $LaFeO_3$/biochar with abundant defect oxygen and functional groups through the co-pyrolysis of lotus and Fe/La salts (Fig. 17a). The presence of OVs in the resulting structure was confirmed through XPS analysis, with the O 1s spectra displaying a peak at 531.2 eV corresponding to OVs. In comparison to pristine $LaFeO_3$ (28.2% content), C–$LaFeO_3$/biochar-2.0 exhibited a higher concentration of defect oxygen (52.9%) due to the incorporation of carbon (C-doping). The findings indicated that the lotus had an impact on both Fe^{3+} and La^{3+}, leading to alterations in the surface and structural properties of the catalysts. The presence of precursor salts (Fe/La) played a role in modifying the biochar surface during carbonization, resulting in enhanced exposure of oxygen functionalities and aromatic moieties, thereby facilitating the adsorption of NO_3^- (Fig. 17b). The involvement of these organic functional groups was vital in promoting the transfer of photogenerated electrons, leading to a favorable preference for donating electrons specifically to ammonium ions (NH_4^+) (Fig. 17c). When exposed to visible light, the $LaFeO_3$/biochar photocatalyst demonstrated remarkable effectiveness, achieving an impressive 98% conversion

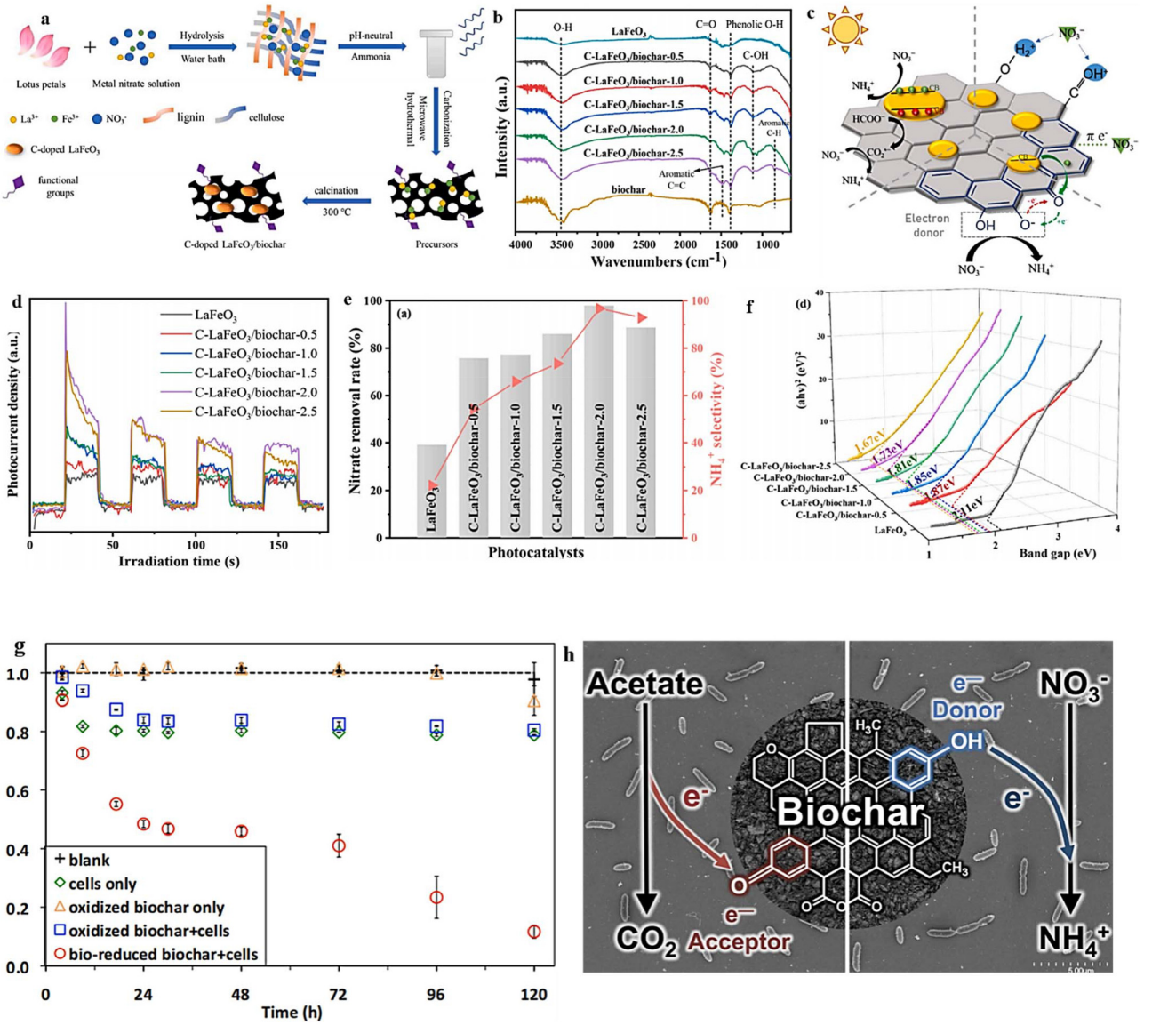

Fig. 17 (a) Schematic depiction of the synthesis route for C–$LaFeO_3$/biochar. (b) Comparative FT-IR analysis of $LaFeO_3$ and C–$LaFeO_3$/biochar. (c) Photocatalytic NO_3^- reduction on C-doped $LaFeO_3$/biochar. (d) Photocurrent as a function of irradiation time, (e) NO_3^- conversion and NH_4^+ selectivity. (f) Respective band gaps of the studied materials. Reproduced from ref. 206 with permission from Elsevier, copyright 2022. (g) NO_3^- reduction in the presence of different conditions: the medium alone (blank), cells only, oxidized biochar in the presence and absence of cells, and biologically reduced biochar plus cells and (h) schematic presentation of the donor group in the reduced biochar. Reproduced from ref. 209 with permission from ACS, copyright 2016.

rate of nitrate and an exceptional 97% selectivity towards NH_3. The utilization of photocurrent response as a reliable method to evaluate the capacity for generating and transferring photo-excited charge carriers under irradiation is demonstrated in (Fig. 17d). The C–$LaFeO_3$/biochar composites exhibited significantly higher photocurrent density compared to pristine $LaFeO_3$, indicating the efficient migration and separation of electron–hole pairs. This further confirms the enhanced performance of C–$LaFeO_3$/biochar composites in harnessing light energy. Additionally, among the C–$LaFeO_3$/biochar and pristine $LaFeO_3$, the C–$LaFeO_3$/biochar-2.0 displayed a reduced resistance to charge transfer. This discovery suggests that the existence of OVs and the robust association between biochar and $LaFeO_3$ particles significantly amplified the speed at which charge carriers migrate.[207,208] Additionally, the composite material synthesized through the biological route exhibited a decreased bandgap in comparison to pristine $LaFeO_3$. Experimental results revealed that pristine $LaFeO_3$ possesses a bandgap of 2.11 eV. However, the C-doped $LaFeO_3$/biochar samples displayed bandgaps ranging from 1.67 to 1.87 eV, indicating an enhanced light absorption capacity of the prepared material within the visible light range (Fig. 17f). The

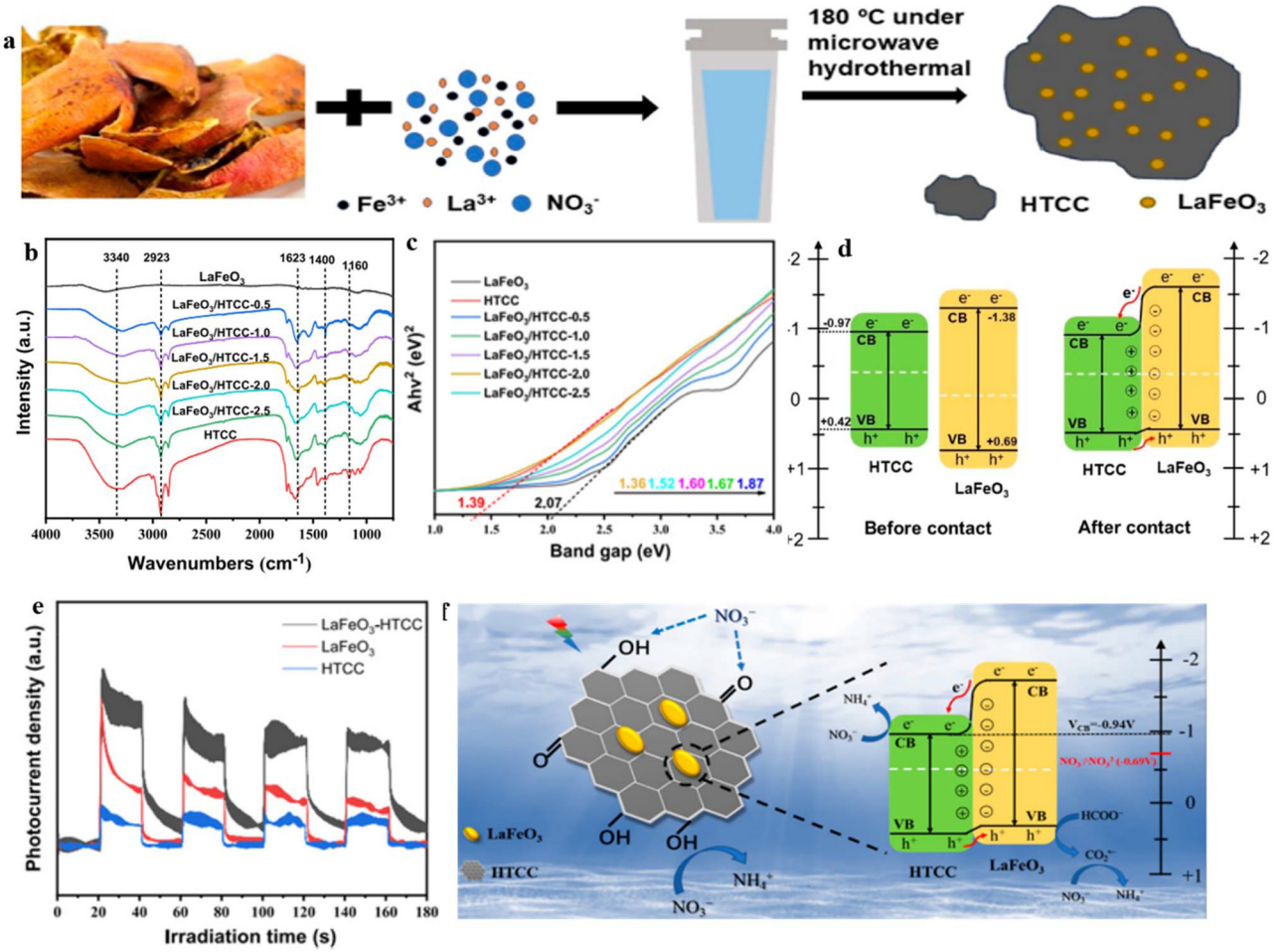

Fig. 18 (a) Illustration depicting the synthesis procedure of the $LaFeO_3$/HTCC. (b) Comparative FT-IR investigation of different materials (pristine $LaFeO_3$, HTCC, and $LaFeO_3$/HTCC-0.5–2.5). (c) Tauc plots, (d) band gap structure of pristine $LaFeO_3$ and HTCC. (e) Photocurrent pattern of the selected materials. (f) Diagram illustrating the photocatalytic conversion process of NO_3^- using the $LaFeO_3$/HTCC composite. Reproduced from ref. 211 with permission from ACS, copyright 2023.

removal capacity of NO_3^- by the material exhibited a direct correlation with the increasing concentration of biochar, up to a certain threshold. However, beyond this limit, a decrease in activity was observed (Fig. 17e). Remarkably, C–$LaFeO_3$/biochar-2.0 exhibited the highest performance, achieving a NO_3^- rate of 98% and a remarkable NH_4^+ selectivity of 97% after 120 minutes. The enhanced selectivity towards NH_4^+ observed in the composites (C-doped $LaFeO_3$/biochar) could potentially be attributed to the presence of reducing groups (phenolic hydroxyl groups) on the surface of biochar. These groups can selectively reduce nitrate to ammonia, as proposed by Saquing *et al.* in 2016 (Fig. 17g and h).[209]

The recombination of photogenerated electron holes poses a significant challenge in photocatalysis, and researchers have consistently worked to address this issue. One promising method to enhance the photocatalytic efficiency of the catalyst is by creating p–n heterojunctions. These junctions effectively improve the separation efficiency of photogenerated electron–hole pairs, resulting in enhanced visible light absorption and heightened catalytic performance.[210] In this regard, Wei and colleagues[211] conducted a study where they utilized pomegranate peel to perform a green synthesis of $LaFeO_3$/HTCC ($LaFeO_3$/hydrothermal carbonation carbon) nanostructured composites *via* the hydrothermal method (Fig. 18a). The resulting biogenic materials demonstrated a high content of oxygen defects (XPS analysis) and bioactive functional groups (FTIR) investigation in (Fig. 18b). These newly designed composites were then evaluated for their catalytic efficiency in the photoelectrochemical conversion of NO_3^- into NH_3. The strategy employed in this study effectively modified the band gap of the p-type $LaFeO_3$ (2.07 eV) by incorporating the n-type organic HTCC (1.39 eV), as demonstrated by the corresponding band gaps shown in (Fig. 18c). A thorough examination of the band structure of both materials, $LaFeO_3$ and HTCC, reveals V_{Vb} values of 0.69 V and 0.42 V, along with corresponding V_{CB} values of −1.38 V and −0.79 V for $LaFeO_3$ and HTCC, respectively. Upon combination, a built-in electric field is created, causing a transfer of a negative charge toward the $LaFeO_3$ side

and a positive charge toward the HTCC side (Fig. 18d). As a result of this distinct charge distribution, an electron–hole pair system is formed, where electrons in the conduction band (CB) move towards HTCC, while holes in the valence band (VB) transfer to $LaFeO_3$ when exposed to visible light. Under the influence of visible light, the photocatalyst synthesized using green methods demonstrated outstanding performance, achieving a NO_3^- removal rate of 94.6% and an impressive NH_3 selectivity of 88.7%. This remarkable efficiency can be attributed to two key factors: the swift separation of photogenerated electron–hole pairs and the abundance of reducing functionalities that act as a green source of electron donors (Fig. 18f).[212,213]

6. Conclusions and perspectives

Recent advancements in electrocatalytic NO_3^- reduction show significant promise in enhancing the efficiency, affordability, and environmental impact of water NO_3^- management. This progress offers the potential to convert NO_3^- contaminants into valuable ammonia products. While extensive research has explored various materials for electrochemical NO_3^- conversion, there is limited investigation into the role of perovskite oxides in this process. This paper aims to address this gap by examining the catalytic relevance of perovskite oxides and strategies for enhancing their electronic structure, covalent properties, and catalytic efficiency. This review provides an up-to-date overview of the electrocatalytic NO_3^- reduction to NH_3 using various perovskite oxide materials. Based on previous experimental and theoretical studies, key factors such as A/B-site cation composition, oxygen vacancy concentration, crystal structure, and electrical conductivity have been identified as crucial determinants of perovskite catalytic performance. A/B-site cations significantly influence the electronic structure, impacting both conductivity and catalytic activity. Oxygen defects impact the electronic arrangement and surface configuration, promoting charge transfer and influencing intermediate binding in chemical reactions. Understanding the correlation between perovskite electronic structure and catalysis has enhanced our ability to design catalysts for important reactions. Meticulous control of A/B cations and oxygen vacancies in perovskite structures could lead to advanced electrocatalysts with improved performance and selectivity in NO_3^- to ammonia conversion. However, challenges remain in deploying perovskite oxides with exceptional electrocatalytic performance in practical applications.

6.1. Creating novel perovskite-based electrocatalysts

Though perovskite oxides show promise in catalysis, their activity often lags behind noble-metal catalysts. Establishing essential criteria linking crystal structure and activity is crucial for designing effective catalysts. While various activity indicators exist, a universally applicable reactivity descriptor is still lacking. Descriptors related to hydrogen evolution and redox reactions are gaining attention and require further exploration. The integration of high-throughput calculations, artificial intelligence, and machine learning can greatly enhance the efficiency of catalyst design and resource utilization.

6.2. Catalytic reaction mechanisms

Further research is needed to fully understand the potential of perovskite materials as catalysts, particularly in redox reactions and the HER. The formation of an amorphous layer on the perovskite surface under inert or reducing conditions complicates their catalytic behavior. While some studies suggest the negative effects of this amorphous phase on catalytic activity, others indicate potential benefits, especially in ORR and OER reactions. Advanced experimental techniques and a deeper understanding of perovskites with amorphous phases are necessary for future exploration.

6.3. Employing a synergistic impact

The performance of an electrocatalyst is influenced by factors such as morphology, conductivity, and surface structure. Depending solely on one design approach restricts performance improvements. Maximizing efficiency requires integrating synergistic effects from multiple design approaches. This typically involves optimizing morphology to increase the number of active sites and adjusting cation ions to enhance activity. Future development will emphasize defect engineering and surface modification for additional enhancements. Controlled surface modification and the creation of oxygen vacancies can enhance the catalytic performance of perovskite-based catalysts.

6.4. Pursuing real-world applications

Creating perovskite oxides with consistent particle sizes and specific surface areas for industrial-scale production remains challenging despite advancements in methodologies. The lack of reliable techniques hinders the widespread use of novel perovskite variants like hollow and core–shell structures. Current durability assessment methods rely on short-term testing data, limiting accurate long-term performance evaluation. Catalysts capable of higher current densities and broader temperature ranges are needed for real-world applications. Perovskite electronic structure is significantly influenced by electrode preparation, requiring high catalyst loading for optimal performance and stability. Perovskite catalysts exhibiting high loadings and homogeneous distributions demonstrate considerable promise for augmenting the efficiency and durability of electrochemical devices, thereby underscoring the imperative for scalable synthesis and mass production of these advanced materials. Industrial-scale production of nanostructured perovskite oxides for nitrate reduction poses significant challenges.[214] A multidisciplinary approach combining experiment, computation, and characterization is crucial for successful implementation.

6.4.1. Working potential and pH. Efforts are ongoing to broaden the applicability of perovskite-structured electrocata-

lysts beyond alkaline environments by exploring their performance in acidic conditions. Achieving universal pH compatibility would greatly enhance their practical utility. However, challenges remain, particularly concerning stability and activity across the pH spectrum. Incorporating carbon can enhance performance but may suffer from electrochemical oxidation, reducing active site availability. Research efforts are also focused on developing novel catalysts with high mixed ionic-electronic conductivity and corrosion resistance as alternatives to carbon-based supports.

6.5. Investigation of interfaces

Understanding catalytic interfaces is a key area of ongoing research, focusing on optimizing electronic charge transfer to enhance catalytic performance. However, unexpected interfaces may pose challenges such as increased resistance, hindering charge transfer efficiency. Thoroughly analyzing established interfaces requires case-specific examinations. Connecting structure with electrocatalytic performance is crucial for developing high-performance catalysts.

6.6. Stability of the catalyst

Ensuring the stability of perovskite oxide catalysts is crucial for practical applications. However, research suggests that perovskite oxides may exhibit lower stability compared to other oxide materials.[215] Techniques aimed at improving catalytic efficiency by increasing oxygen vacancies and electrical conductivity could compromise stability. Additionally, changes like surface reconstruction occurring within perovskite oxides during catalytic processes may further reduce stability. Therefore, gaining a deeper understanding of perovskite oxide catalyst stability is essential. Novel techniques are being explored to develop perovskite oxide-based catalysts with improved activity and stability.

6.7. Precise manipulation and quantitative analysis of site vacancies

Most research has focused qualitatively on how different site vacancies enhance catalytic performance, with limited quantitative inquiries due to the challenging task of analyzing active vacancy centers using traditional methods. Developing innovative *in situ* characterization techniques is crucial for comprehensive investigations of ABO_3 catalysts with distinct vacancy states, both during sample preparation and catalytic reactions. Additionally, precise thermodynamic and kinetic simulations can predictively identify the significant contribution of vacancy sites in various catalytic reactions involving ABO_3 catalysts, guiding further advancements in catalyst development.

Data availability

The data findings of this review are available from the corresponding authors upon reasonable request.

Conflicts of interest

The authors declared that there is no conflict of interest.

Acknowledgements

The authors acknowledge financial support from the Construction Project of Nano Technology and Application Engineering Research Center of Guangdong Medical University (No. 4SG24179G), Guangdong Basic and Applied Basic Research Foundation (No. 2022A1515110158, 2024A1515012577), the National Natural Science Foundation of China (No. 32300048).

References

1 Y. Ashida, K. Arashiba, K. Nakajima and Y. Nishibayashi, Molybdenum-catalysed ammonia production with samarium diiodide and alcohols or water, *Nature*, 2019, **568**, 536–540.
2 R. F. Service, New recipe produces ammonia from air, water, and sunlight, *Science*, 2014, **345**, 610.
3 C. Tang and S.-Z. Qiao, How to explore ambient electrocatalytic nitrogen reduction reliably and insightfully, *Chem. Soc. Rev.*, 2019, **48**, 3166–3180.
4 X. Fu, J. B. Pedersen, Y. Zhou, M. Saccoccio, S. Li, R. Sažinas, K. Li, S. Z. Andersen, A. Xu and N. H. Deissler, Continuous-flow electrosynthesis of ammonia by nitrogen reduction and hydrogen oxidation, *Science*, 2023, **379**, 707–712.
5 D. Ye and S. C. E. Tsang, Prospects and challenges of green ammonia synthesis, *Nat. Synth.*, 2023, 1–12.
6 G. Soloveichik, Electrochemical synthesis of ammonia as a potential alternative to the Haber–Bosch process, *Nat. Catal.*, 2019, **2**, 377–380.
7 R. Hawtof, S. Ghosh, E. Guarr, C. Xu, R. Mohan Sankaran and J. N. Renner, Catalyst-free, highly selective synthesis of ammonia from nitrogen and water by a plasma electrolytic system, *Sci. Adv.*, 2019, **5**, eaat5778.
8 S. L. Foster, S. I. P. Bakovic, R. D. Duda, S. Maheshwari, R. D. Milton, S. D. Minteer, M. J. Janik, J. N. Renner and L. F. Greenlee, Catalysts for nitrogen reduction to ammonia, *Nat. Catal.*, 2018, **1**, 490–500.
9 Y. Song, D. Johnson, R. Peng, D. K. Hensley, P. V. Bonnesen, L. Liang, J. Huang, F. Yang, F. Zhang and R. Qiao, A physical catalyst for the electrolysis of nitrogen to ammonia, *Sci. Adv.*, 2018, **4**, e1700336.
10 P. Song, L. Kang, H. Wang, R. Guo and R. Wang, Nitrogen (N), phosphorus (P)-codoped porous carbon as a metal-free electrocatalyst for N2 reduction under ambient conditions, *ACS Appl. Mater. Interfaces*, 2019, **11**, 12408–12414.
11 T. Brown, What drives new investments in low-carbon ammonia production? One million tons per day demand,

Ammonia-Industry. com, https://ammoniaindustry.com/what-drives-newinvestments-in-low-carbon-ammonia (Apr. 2018).
12 R. F. Service, Ammonia-a renewable fuel made from sun, air, and water—could power the globe without carbon, *Science*, 2018, DOI: 10.1126/science.aau7489.
13 Z. W. Seh, J. Kibsgaard, C. F. Dickens, I. Chorkendorff, J. K. Nørskov and T. F. Jaramillo, Combining theory and experiment in electrocatalysis: Insights into materials design, *Science*, 2017, **355**, eaad4998.
14 K. Chen, D. Ma, Y. Zhang, F. Wang, X. Yang, X. Wang, H. Zhang, X. Liu, R. Bao and K. Chu, Urea electrosynthesis from nitrate and CO2 on diatomic alloys, *Adv. Mater.*, 2024, **36**, 2402160.
15 S. Chen, G. Qi, R. Yin, Q. Liu, L. Feng, X. Feng, G. Hu, J. Luo, X. Liu and W. Liu, Electrocatalytic nitrate-to-ammonia conversion on CoO/CuO nanoarrays using Zn–nitrate batteries, *Nanoscale*, 2023, **15**, 19577–19585.
16 A. N. Singh, R. Anand, M. Zafari, M. Ha and K. S. Kim, Progress in single/multi atoms and 2D–nanomaterials for electro/photocatalytic nitrogen reduction: experimental, computational and machine leaning developments, *Adv. Energy Mater.*, 2024, 2304106.
17 G.-F. Chen, X. Cao, S. Wu, X. Zeng, L.-X. Ding, M. Zhu and H. Wang, Ammonia electrosynthesis with high selectivity under ambient conditions via a Li+ incorporation strategy, *J. Am. Chem. Soc.*, 2017, **139**, 9771–9774.
18 Q. Gao, B. Yao, H. S. Pillai, W. Zang, X. Han, Y. Liu, S.-W. Yu, Z. Yan, B. Min and S. Zhang, Synthesis of core/shell nanocrystals with ordered intermetallic single-atom alloy layers for nitrate electroreduction to ammonia, *Nat. Synth.*, 2023, 1–11.
19 S. Han, H. Li, T. Li, F. Chen, R. Yang, Y. Yu and B. Zhang, Ultralow overpotential nitrate reduction to ammonia via a three-step relay mechanism, *Nat. Catal.*, 2023, 1–13.
20 G. Zhang, G. Wang, Y. Wan, X. Liu and K. Chu, Ampere-level nitrate electroreduction to ammonia over monodispersed Bi-doped FeS2, *ACS Nano*, 2023, **17**, 21328–21336.
21 C. Lv, C. Yan, G. Chen, Y. Ding, J. Sun, Y. Zhou and G. Yu, An amorphous noble–metal–free electrocatalyst that enables nitrogen fixation under ambient conditions, *Angew. Chem.*, 2018, **130**, 6181–6184.
22 X. Chen, Y. Guo, X. Du, Y. Zeng, J. Chu, C. Gong, J. Huang, C. Fan, X. Wang and J. Xiong, Atomic structure modification for electrochemical nitrogen reduction to ammonia, *Adv. Energy Mater.*, 2020, **10**, 1903172.
23 B. H. Suryanto, K. Matuszek, J. Choi, R. Y. Hodgetts, H.-L. Du, J. M. Bakker, C. S. Kang, P. V. Cherepanov, A. N. Simonov and D. R. MacFarlane, Nitrogen reduction to ammonia at high efficiency and rates based on a phosphonium proton shuttle, *Science*, 2021, **372**, 1187–1191.
24 W. Lin, H. Chen, G. Lin, S. Yao, Z. Zhang, J. Qi, M. Jing, W. Song, J. Li and X. Liu, Creating frustrated lewis pairs in defective boron carbon nitride for electrocatalytic nitrogen reduction to ammonia, *Angew. Chem., Int. Ed.*, 2022, **61**, e202207807.
25 H.-L. Du, M. Chatti, R. Y. Hodgetts, P. V. Cherepanov, C. K. Nguyen, K. Matuszek, D. R. MacFarlane and A. N. Simonov, Electroreduction of nitrogen with almost 100% current-to-ammonia efficiency, *Nature*, 2022, **609**, 722–727.
26 S. Zhang, M. Han, T. Shi, H. Zhang, Y. Lin, X. Zheng, L. R. Zheng, H. Zhou, C. Chen and Y. Zhang, Atomically dispersed bimetallic Fe–Co electrocatalysts for green production of ammonia, *Nat. Sustain.*, 2023, **6**, 169–179.
27 B. H. Suryanto, H.-L. Du, D. Wang, J. Chen, A. N. Simonov and D. R. MacFarlane, Challenges and prospects in the catalysis of electroreduction of nitrogen to ammonia, *Nat. Catal.*, 2019, **2**, 290–296.
28 J. Deng, J. A. Iñiguez and C. Liu, Electrocatalytic nitrogen reduction at low temperature, *Joule*, 2018, **2**, 846–856.
29 Y. Ren, C. Yu, L. Wang, X. Tan, Z. Wang, Q. Wei, Y. Zhang and J. Qiu, Microscopic-Level Insights into the Mechanism of Enhanced NH3 Synthesis in Plasma-Enabled Cascade N2 Oxidation–Electroreduction System, *J. Am. Chem. Soc.*, 2022, **144**, 10193–10200.
30 S. Z. Andersen, V. Čolić, S. Yang, J. A. Schwalbe, A. C. Nielander, J. M. McEnaney, K. Enemark-Rasmussen, J. G. Baker, A. R. Singh and B. A. Rohr, A rigorous electrochemical ammonia synthesis protocol with quantitative isotope measurements, *Nature*, 2019, **570**, 504–508.
31 J. Choi, B. H. Suryanto, D. Wang, H.-L. Du, R. Y. Hodgetts, F. M. Ferrero Vallana, D. R. MacFarlane and A. N. Simonov, Identification and elimination of false positives in electrochemical nitrogen reduction studies, *Nat. Commun.*, 2020, **11**, 5546.
32 Y. Zeng, C. Priest, G. Wang and G. Wu, Restoring the nitrogen cycle by electrochemical reduction of nitrate: progress and prospects, *Small Methods*, 2020, **4**, 2000672.
33 Y. Li, Q. Zhang, Z. Mei, S. Li, W. Luo, F. Pan, H. Liu and S. Dou, Recent advances and perspective on electrochemical ammonia synthesis under ambient conditions, *Small Methods*, 2021, **5**, 2100460.
34 J. M. McEnaney, S. J. Blair, A. C. Nielander, J. A. Schwalbe, D. M. Koshy, M. Cargnello and T. F. Jaramillo, Electrolyte engineering for efficient electrochemical nitrate reduction to ammonia on a titanium electrode, *ACS Sustainable Chem. Eng.*, 2020, **8**, 2672–2681.
35 G.-F. Chen, Y. Yuan, H. Jiang, S.-Y. Ren, L.-X. Ding, L. Ma, T. Wu, J. Lu and H. Wang, Electrochemical reduction of nitrate to ammonia via direct eight-electron transfer using a copper–molecular solid catalyst, *Nat. Energy*, 2020, **5**, 605–613.
36 P. H. van Langevelde, I. Katsounaros and M. T. Koper, Electrocatalytic nitrate reduction for sustainable ammonia production, *Joule*, 2021, **5**, 290–294.
37 J. O. Lundberg, E. Weitzberg, J. A. Cole and N. Benjamin, Nitrate, bacteria and human health, *Nat. Rev. Microbiol.*, 2004, **2**, 593–602.
38 S. Garcia-Segura, M. Lanzarini-Lopes, K. Hristovski and P. Westerhoff, Electrocatalytic reduction of nitrate: Fundamentals to full-scale water treatment applications, *Appl. Catal., B*, 2018, **236**, 546–568.

39 A. A. Avery, Infantile methemoglobinemia: reexamining the role of drinking water nitrates, *Environ. Health Perspect.*, 1999, **107**, 583–586.
40 H. Liu, X. Lang, C. Zhu, J. Timoshenko, M. Rüscher, L. Bai, N. Guijarro, H. Yin, Y. Peng and J. Li, Efficient Electrochemical Nitrate Reduction to Ammonia with Copper–Supported Rhodium Cluster and Single–Atom Catalysts, *Angew. Chem.*, 2022, **134**, e202202556.
41 S. Zhang, J. Wu, M. Zheng, X. Jin, Z. Shen, Z. Li, Y. Wang, Q. Wang, X. Wang and H. Wei, Fe/Cu diatomic catalysts for electrochemical nitrate reduction to ammonia, *Nat. Commun.*, 2023, **14**, 3634.
42 F.-Y. Chen, Z.-Y. Wu, S. Gupta, D. J. Rivera, S. V. Lambeets, S. Pecaut, J. Y. T. Kim, P. Zhu, Y. Z. Finfrock and D. M. Meira, Efficient conversion of low-concentration nitrate sources into ammonia on a Ru-dispersed Cu nanowire electrocatalyst, *Nat. Nanotechnol.*, 2022, **17**, 759–767.
43 W. Song, L. Yue, X. Fan, Y. Luo, B. Ying, S. Sun, D. Zheng, Q. Liu, M. S. Hamdy and X. Sun, Recent progress and strategies on design of catalysts for electrochemical ammonia synthesis from nitrate reduction, *Inorg. Chem. Front.*, 2023, **10**, 3489–3514.
44 M. Yang, T. Wei, J. He, Q. Liu, L. Feng, H. Li, J. Luo and X. Liu, Au nanoclusters anchored on TiO2 nanosheets for high-efficiency electroreduction of nitrate to ammonia, *Nano Res.*, 2024, **17**, 1209–1216.
45 H. Xu, Y. Ma, J. Chen, W.-x. Zhang and J. Yang, Electrocatalytic reduction of nitrate–a step towards a sustainable nitrogen cycle, *Chem. Soc. Rev.*, 2022, **51**, 2710–2758.
46 X. Zou, J. Xie, C. Wang, G. Jiang, K. Tang and C. Chen, Electrochemical nitrate reduction to produce ammonia integrated into wastewater treatment: Investigations and challenges, *Chin. Chem. Lett.*, 2023, **34**, 107908.
47 W. Jung and Y. J. Hwang, Material strategies in the electrochemical nitrate reduction reaction to ammonia production, *Mater. Chem. Front.*, 2021, **5**, 6803–6823.
48 Y. Li, Y. K. Go, H. Ooka, D. He, F. Jin, S. H. Kim and R. Nakamura, Enzyme mimetic active intermediates for nitrate reduction in neutral aqueous media, *Angew. Chem., Int. Ed.*, 2020, **59**, 9744–9750.
49 E. Pérez-Gallent, M. C. Figueiredo, I. Katsounaros and M. T. Koper, Electrocatalytic reduction of Nitrate on Copper single crystals in acidic and alkaline solutions, *Electrochim. Acta*, 2017, **227**, 77–84.
50 S. Ullah, S. Wang, M. S. Ahmad, H. M. A. Sharif, Q. Liu, T. Kida, A. Shafique, M. U. Rehman, G. Wang and J. Qiu, Investigating the role of oxygen vacancies in metal oxide for enhanced electrochemical reduction of NO 3− to NH 3: mechanistic insights, *Inorg. Chem. Front.*, 2023, **10**, 6440–6488.
51 S. Ullah, S. Wang, C. Li, A. U. Jan, F. Zhan, H. M. A. Sharif, Q. Liu and G. Wang, Recent developments in designing Cu-based electrocatalysts and advanced strategies for electrochemical nitrate reduction to ammonia, *J. Environ. Chem. Eng.*, 2023, 110927.
52 Q. Peng, D. Xing, L. Dong, Y. Fu, J. Lu, X. Wang, C. Wang and C. Guo, Electrochemical nitrate reduction for ammonia production: amorphous or crystalline oxidized copper catalyst?, *J. Mater. Chem. A*, 2024, **12**, 8689–8693.
53 Z. Yao, J. Yao, H. Luo, Y. Chen, J. Hu, F. Du and C. Guo, Cu/Ni (OH) 2 nanocomposites for efficient and stable electrocatalysis nitrate reduction reaction to ammonia, *Mater. Lett.*, 2024, **364**, 136324.
54 T. Hu, M. Wang, L. Ren, C. M. Li and C. Guo, Local Chemical Environment Dependent Nitrate-Reduction-to-Ammonia Performance on Cu-Based Electrocatalysts, *J. Phys. Chem. Lett.*, 2024, **15**, 3258–3266.
55 L. Zhang, L. Wang, H. Lin, Y. Liu, J. Ye, Y. Wen, A. Chen, L. Wang, F. Ni and Z. Zhou, A lattice–oxygen–involved reaction pathway to boost urea oxidation, *Angew. Chem.*, 2019, **131**, 16976–16981.
56 Z. Geng, X. Kong, W. Chen, H. Su, Y. Liu, F. Cai, G. Wang and J. Zeng, Oxygen vacancies in ZnO nanosheets enhance CO2 electrochemical reduction to CO, *Angew. Chem.*, 2018, **130**, 6162–6167.
57 R. Jia, Y. Wang, C. Wang, Y. Ling, Y. Yu and B. Zhang, Boosting selective nitrate electroreduction to ammonium by constructing oxygen vacancies in TiO2, *ACS Catal.*, 2020, **10**, 3533–3540.
58 J. Lin, T. Huang, M. Lu, X. Lin, R. C. K. Reddy and X. Xu, Modulating electronic structure of metal-organic frameworks derived zinc manganates by oxygen vacancies for superior lithium storage, *Chem. Eng. J.*, 2022, **433**, 133770.
59 M. K. Bruska, I. Czekaj, B. Delley, J. Mantzaras and A. Wokaun, Electronic structure and oxygen vacancies in PdO and ZnO: validation of DFT models, *Phys. Chem. Chem. Phys.*, 2011, **13**, 15947–15954.
60 Y. Xu, K. Ren, T. Ren, M. Wang, Z. Wang, X. Li, L. Wang and H. Wang, Ultralow-content Pd *in situ* incorporation mediated hierarchical defects in corner-etched Cu2O octahedra for enhanced electrocatalytic nitrate reduction to ammonia, *Appl. Catal., B*, 2022, **306**, 121094.
61 Y. Zhu, L. Zhang, B. Zhao, H. Chen, X. Liu, R. Zhao, X. Wang, J. Liu, Y. Chen and M. Liu, Improving the activity for oxygen evolution reaction by tailoring oxygen defects in double perovskite oxides, *Adv. Funct. Mater.*, 2019, **29**, 1901783.
62 C. Sun, J. A. Alonso and J. Bian, Recent advances in perovskite–type oxides for energy conversion and storage applications, *Adv. Energy Mater.*, 2021, **11**, 2000459.
63 J. Zhu, H. Li, L. Zhong, P. Xiao, X. Xu, X. Yang, Z. Zhao and J. Li, Perovskite oxides: preparation, characterizations, and applications in heterogeneous catalysis, *ACS Catal.*, 2014, **4**, 2917–2940.
64 T. Ishihara, Structure and properties of perovskite oxides, *Perovskite Oxide for Solid Oxide Fuel Cells*, 2009, pp. 1–16.
65 Q. Ji, L. Bi, J. Zhang, H. Cao and X. S. Zhao, The role of oxygen vacancies of ABO 3 perovskite oxides in the oxygen reduction reaction, *Energy Environ. Sci.*, 2020, **13**, 1408–1428.
66 H. Zhang, Y. Xu, M. Lu, X. Xie and L. Huang, Perovskite Oxides for Cathodic Electrocatalysis of Energy–Related

Gases: From O2 to CO2 and N2, *Adv. Funct. Mater.*, 2021, **31**, 2101872.

67 C. J. Bartel, C. Sutton, B. R. Goldsmith, R. Ouyang, C. B. Musgrave, L. M. Ghiringhelli and M. Scheffler, New tolerance factor to predict the stability of perovskite oxides and halides, *Sci. Adv.*, 2019, **5**, eaav0693.

68 J. Hwang, R. R. Rao, L. Giordano, Y. Katayama, Y. Yu and Y. Shao-Horn, Perovskites in catalysis and electrocatalysis, *Science*, 2017, **358**, 751–756.

69 C. Sun, J. A. Alonso and J. Bian, Recent Advances in Perovskite-Type Oxides for Energy Conversion and Storage Applications, *Adv. Energy Mater.*, 2021, **11**, 2000459.

70 J. Simböck, M. Ghiasi, S. Schönebaum, U. Simon, F. M. F. de Groot and R. Palkovits, Electronic parameters in cobalt-based perovskite-type oxides as descriptors for chemocatalytic reactions, *Nat. Commun.*, 2020, **11**, 652.

71 K. Wang, C. Han, Z. Shao, J. Qiu, S. Wang and S. Liu, Perovskite oxide catalysts for advanced oxidation reactions, *Adv. Funct. Mater.*, 2021, **31**, 2102089.

72 Y. Cao, J. Liang, X. Li, L. Yue, Q. Liu, S. Lu, A. M. Asiri, J. Hu, Y. Luo and X. Sun, Recent advances in perovskite oxides as electrode materials for supercapacitors, *Chem. Commun.*, 2021, **57**, 2343–2355.

73 Y. Wu, L. Li, B. Chu, Y. Yi, Z. Qin, M. Fan, Q. Qin, H. He, L. Zhang and L. Dong, Catalytic reduction of NO by CO over B-site partially substituted LaM0. 25Co0. 75O3 (M = Cu, Mn, Fe) perovskite oxide catalysts: The correlation between physicochemical properties and catalytic performance, *Appl. Catal., A*, 2018, **568**, 43–53.

74 K. Chu, F. Liu, J. Zhu, H. Fu, H. Zhu, Y. Zhu, Y. Zhang, F. Lai and T. Liu, A general strategy to boost electrocatalytic nitrogen reduction on perovskite oxides via the oxygen vacancies derived from a–site deficiency, *Adv. Energy Mater.*, 2021, **11**, 2003799.

75 X. Zhang, E. A. Davidson, D. L. Mauzerall, T. D. Searchinger, P. Dumas and Y. Shen, Managing nitrogen for sustainable development, *Nature*, 2015, **528**, 51–59.

76 L. Lin, S. St Clair, G. D. Gamble, C. A. Crowther, L. Dixon, F. H. Bloomfield and J. E. Harding, Nitrate contamination in drinking water and adverse reproductive and birth outcomes: a systematic review and meta-analysis, *Sci. Rep.*, 2023, **13**, 563.

77 J. D. Brender, Human health effects of exposure to nitrate, nitrite, and nitrogen dioxide, *Just enough nitrogen: Perspectives on how to get there for regions with too much and too little nitrogen*, 2020, pp. 283–294.

78 D. Jain, P. Chaudhary, N. Varshney and P. Janmeda, Carcinogenic effects of N-nitroso compounds in the environment, *Environ. Conserv. J.*, 2020, **21**, 25–41.

79 K. Iijima, E. Henry, A. Moriya, A. Wirz, A. Kelman and K. McColl, Dietary nitrate generates potentially mutagenic concentrations of nitric oxide at the gastroesophageal junction, *Gastroenterology*, 2002, **122**, 1248–1257.

80 K. Iijima, J. Grant, K. McElroy, V. Fyfe, T. Preston and K. E. McColl, Novel mechanism of nitrosative stress from dietary nitrate with relevance to gastro-oesophageal junction cancers, *Carcinogenesis*, 2003, **24**, 1951–1960.

81 J. Khatri, C. E. Mills, P. Maskell, C. Odongerel and A. J. Webb, It is rocket science–why dietary nitrate is hard to 'beet'! Part I: twists and turns in the realization of the nitrate–nitrite–NO pathway, *Br. J. Clin. Pharmacol.*, 2017, **83**, 129–139.

82 H. Bartsch, H. Ohshima and B. Pignatelli, Inhibitors of endogenous nitrosation mechanisms and implications in human cancer prevention, *Mutat. Res., Fundam. Mol. Mech. Mutagen.*, 1988, **202**, 307–324.

83 A. Mohsen, A. Hassan, S. M. El-Sewedy, T. Aboul-Azm, C. Magagnotti, R. Fanelli and L. Airoldi, Human bladder cancer, schistosomiasis, N-nitroso compounds and their precursors, *Int. J. Cancer*, 2000, **88**, 682–683.

84 M. H. Mostafa, S. Sheweita and P. O'Connor, Relationship between schistosomiasis and bladder cancer, *Clin. Microbiol. Rev.*, 1999, **12**, 97–111.

85 A. F. Badawi, Nitrate, nitrite and N-nitroso compounds in human bladder cancer associated with schistosomiasis, *Int. J. Cancer*, 2000, **86**, 598–600.

86 S. F. Johnson, Methemoglobinemia: Infants at risk, *Curr. Probl. Pediatr. Adolesc. Health Care*, 2019, **49**, 57–67.

87 N. Patel, A. L. Srivastav, A. Patel, A. Singh, S. K. Singh, V. K. Chaudhary, P. K. Singh and B. Bhunia, Nitrate contamination in water resources, human health risks and its remediation through adsorption: a focused review, *Environ. Sci. Pollut. Res.*, 2022, **29**, 69137–69152.

88 M. Sadeq, C. L. Moe, B. Attarassi, I. Cherkaoui, R. ElAouad and L. Idrissi, Drinking water nitrate and prevalence of methemoglobinemia among infants and children aged 1–7 years in Moroccan areas, *Int. J. Hyg. Environ. Health*, 2008, **211**, 546–554.

89 M. Tonacchera, A. Pinchera, A. Dimida, E. Ferrarini, P. Agretti, P. Vitti, F. Santini, K. Crump and J. Gibbs, Relative potencies and additivity of perchlorate, thiocyanate, nitrate, and iodide on the inhibition of radioactive iodide uptake by the human sodium iodide symporter, *Thyroid*, 2004, **14**, 1012–1019.

90 B. De Groef, B. R. Decallonne, S. Van der Geyten, V. M. Darras and R. Bouillon, Perchlorate versus other environmental sodium/iodide symporter inhibitors: potential thyroid-related health effects, *Eur. J. Endocrinol.*, 2006, **155**, 17–25.

91 A. Bizhanova and P. Kopp, The sodium-iodide symporter NIS and pendrin in iodide homeostasis of the thyroid, *Endocrinology*, 2009, **150**, 1084–1090.

92 Y. Hiasa, Y. Kitahori, M. Kitamura, H. Nishioka, K. Yane, M. Fukumoto, M. Ohshima, S. Nakaoka and S. Nishii, Relationships between serum thyroid stimulating hormone levels and development of thyroid tumors in rats treated with N-bis-(2-hydroxypropyl) nitrosamine, *Carcinogenesis*, 1991, **12**, 873–877.

93 M. H. Ward, B. A. Kilfoy, P. J. Weyer, K. E. Anderson, A. R. Folsom and J. R. Cerhan, Nitrate intake and the risk

of thyroid cancer and thyroid disease, *Epidemiology*, 2010, **21**, 389–395.

94 B. A. Kilfoy, Y. Zhang, Y. Park, T. R. Holford, A. Schatzkin, A. Hollenbeck and M. H. Ward, Dietary nitrate and nitrite and the risk of thyroid cancer in the NIH–AARP Diet and Health Study, *Int. J. Cancer*, 2011, **129**, 160–172.

95 E. Garcia Torres, R. Perez Morales, A. Gonzalez Zamora, E. Rios Sanchez, E. H. Olivas Calderon, J. d. J. Alba Romero and E. Y. Calleros Rincon, Consumption of water contaminated by nitrate and its deleterious effects on the human thyroid gland: a review and update, *Int. J. Environ. Health Res.*, 2022, **32**, 984–1001.

96 S. J. Joyce, A. Cook, J. Newnham, M. Brenters, C. Ferguson and P. Weinstein, Water disinfection by-products and prelabor rupture of membranes, *Am. J. Epidemiol.*, 2008, **168**, 514–521.

97 A. R. Sherris, M. Baiocchi, S. Fendorf, S. P. Luby, W. Yang and G. M. Shaw, Nitrate in drinking water during pregnancy and spontaneous preterm birth: a retrospective within-mother analysis in California, *Environ. Health Perspect.*, 2021, **129**, 057001.

98 M. H. Ward, R. R. Jones, J. D. Brender, T. M. De Kok, P. J. Weyer, B. T. Nolan, C. M. Villanueva and S. G. Van Breda, Drinking water nitrate and human health: an updated review, *Int. J. Environ. Res. Public Health*, 2018, **15**, 1557.

99 R. Poulsen, N. Cedergreen, T. Hayes and M. Hansen, Nitrate: an environmental endocrine disruptor? A review of evidence and research needs, *Environ. Sci. Technol.*, 2018, **52**, 3869–3887.

100 A. S. Jensen, V. R. Coffman, J. Schullehner, B. B. Trabjerg, C. B. Pedersen, B. Hansen, J. Olsen, M. Pedersen, L. T. Stayner and T. Sigsgaard, Prenatal exposure to tap water containing nitrate and the risk of small-for-gestational-age: A nationwide register-based study of Danish births, 1991–2015, *Environ. Int.*, 2023, **174**, 107883.

101 L. G. Tejuca and J. L. Fierro, *Properties and applications of perovskite-type oxides*, CRC Press, 2000.

102 R. Voorhoeve, D. Johnson Jr, J. Remeika and P. Gallagher, Perovskite Oxides: Materials Science in Catalysis: Perovskite oxides, long known in solid-state chemistry and physics, find new applications in catalysis, *Science*, 1977, **195**, 827–833.

103 J. Xu, C. Chen, Z. Han, Y. Yang, J. Li and Q. Deng, Recent advances in oxygen electrocatalysts based on perovskite oxides, *Nanomaterials*, 2019, **9**, 1161.

104 M. A. Peña and J. Fierro, Chemical structures and performance of perovskite oxides, *Chem. Rev.*, 2001, **101**, 1981–2018.

105 J. Mi, J. Chen, X. Chen, X. Liu and J. Li, Recent Status and Developments of Vacancies Modulation in the ABO3 Perovskites for Catalytic Applications, *Chem. – Eur. J.*, 2023, **29**, e202202713.

106 X. Xu, Y. Zhong and Z. Shao, Double perovskites in catalysis, electrocatalysis, and photo (electro) catalysis, *Trends Chem.*, 2019, **1**, 410–424.

107 W. T. Hong, M. Risch, K. A. Stoerzinger, A. Grimaud, J. Suntivich and Y. Shao-Horn, Toward the rational design of non-precious transition metal oxides for oxygen electrocatalysis, *Energy Environ. Sci.*, 2015, **8**, 1404–1427.

108 J. Zaanen and G. Sawatzky, Systematics in band gaps and optical spectra of 3D transition metal compounds, *J. Solid State Chem.*, 1990, **88**, 8–27.

109 J. Suntivich, H. A. Gasteiger, N. Yabuuchi, H. Nakanishi, J. B. Goodenough and Y. Shao-Horn, Design principles for oxygen-reduction activity on perovskite oxide catalysts for fuel cells and metal–air batteries, *Nat. Chem.*, 2011, **3**, 546–550.

110 J. Suntivich, K. J. May, H. A. Gasteiger, J. B. Goodenough and Y. Shao-Horn, A perovskite oxide optimized for oxygen evolution catalysis from molecular orbital principles, *Science*, 2011, **334**, 1383–1385.

111 A. Grimaud, O. Diaz-Morales, B. Han, W. T. Hong, Y.-L. Lee, L. Giordano, K. A. Stoerzinger, M. T. Koper and Y. Shao-Horn, Activating lattice oxygen redox reactions in metal oxides to catalyse oxygen evolution, *Nat. Chem.*, 2017, **9**, 457–465.

112 J. Suntivich, W. T. Hong, Y.-L. Lee, J. M. Rondinelli, W. Yang, J. B. Goodenough, B. Dabrowski, J. W. Freeland and Y. Shao-Horn, Estimating hybridization of transition metal and oxygen states in perovskites from Ok-edge X-ray absorption spectroscopy, *J. Phys. Chem. C*, 2014, **118**, 1856–1863.

113 D. N. Mueller, M. L. Machala, H. Bluhm and W. C. Chueh, Redox activity of surface oxygen anions in oxygen-deficient perovskite oxides during electrochemical reactions, *Nat. Commun.*, 2015, **6**, 6097.

114 Y.-L. Lee, J. Kleis, J. Rossmeisl, Y. Shao-Horn and D. Morgan, Prediction of solid oxide fuel cell cathode activity with first-principles descriptors, *Energy Environ. Sci.*, 2011, **4**, 3966–3970.

115 G. Lin, Z. Zhang, Q. Ju, T. Wu, C. U. Segre, W. Chen, H. Peng, H. Zhang, Q. Liu and Z. Liu, Bottom-up evolution of perovskite clusters into high-activity rhodium nanoparticles toward alkaline hydrogen evolution, *Nat. Commun.*, 2023, **14**, 280.

116 Y. Zhu, D. Liu, H. Jing, F. Zhang, X. Zhang, S. Hu, L. Zhang, J. Wang, L. Zhang and W. Zhang, Oxygen activation on Ba-containing perovskite materials, *Sci. Adv.*, 2022, **8**, eabn4072.

117 H. Zhang, K. Xu, F. He, Y. Zhou, K. Sasaki, B. Zhao, Y. Choi, M. Liu and Y. Chen, Surface Regulating of a Double–Perovskite Electrode for Protonic Ceramic Fuel Cells to Enhance Oxygen Reduction Activity and Contaminants Poisoning Tolerance, *Adv. Energy Mater.*, 2022, **12**, 2200761.

118 H. Zheng, Y. Zhang, Y. Wang, Z. Wu, F. Lai, G. Chao, N. Zhang, L. Zhang and T. Liu, Perovskites with enriched oxygen vacancies as a family of electrocatalysts for efficient nitrate reduction to ammonia, *Small*, 2023, **19**, 2205625.

119 J. Ran, L. Wang, M. Si, X. Liang and D. Gao, Tailoring Spin State of Perovskite Oxides by Fluorine Atom Doping for Efficient Oxygen Electrocatalysis, *Small*, 2023, **19**, 2206367.

120 Y. Gao, X. Wang, N. Corolla, T. Eldred, A. Bose, W. Gao and F. Li, Alkali metal halide–coated perovskite redox catalysts for anaerobic oxidative dehydrogenation of n-butane, *Sci. Adv.*, 2022, **8**, eabo7343.

121 W. T. Hong, K. A. Stoerzinger, Y.-L. Lee, L. Giordano, A. Grimaud, A. M. Johnson, J. Hwang, E. J. Crumlin, W. Yang and Y. Shao-Horn, Charge-transfer-energy-dependent oxygen evolution reaction mechanisms for perovskite oxides, *Energy Environ. Sci.*, 2017, **10**, 2190–2200.

122 J. D. Benck, T. R. Hellstern, J. Kibsgaard, P. Chakthranont and T. F. Jaramillo, Catalyzing the hydrogen evolution reaction (HER) with molybdenum sulfide nanomaterials, *ACS Catal.*, 2014, **4**, 3957–3971.

123 X. Fu, J. Zhang and Y. Kang, Recent advances and challenges of electrochemical ammonia synthesis, *Chem Catal.*, 2022, **2**, 2590–2613.

124 L. Zhang, L. Wang, Y. Wen, F. Ni, B. Zhang and H. Peng, Boosting neutral water oxidation through surface oxygen modulation, *Adv. Mater.*, 2020, **32**, 2002297.

125 X. Fan, J. Liang, L. Zhang, D. Zhao, L. Yue, Y. Luo, Q. Liu, L. Xie, N. Li and B. Tang, Enhanced electrocatalytic nitrate reduction to ammonia using plasma–induced oxygen vacancies in CoTiO3− x nanofiber, *Carbon Neutralization*, 2022, **1**, 6–13.

126 C. Hu, X. Wang, T. Yao, T. Gao, J. Han, X. Zhang, Y. Zhang, P. Xu and B. Song, Enhanced electrocatalytic oxygen evolution activity by tuning both the oxygen vacancy and orbital occupancy of b–site metal cation in NdNiO3, *Adv. Funct. Mater.*, 2019, **29**, 1902449.

127 Z. Wang, X. Mao, P. Chen, M. Xiao, S. A. Monny, S. Wang, M. Konarova, A. Du and L. Wang, Understanding the roles of oxygen vacancies in hematite–based photoelectrochemical processes, *Angew. Chem.*, 2019, **131**, 1042–1046.

128 Y. Lu, Y. Huang, Y. Zhang, T. Huang, H. Li, J.-j. Cao and W. Ho, Effects of H_2O_2 generation over visible light-responsive Bi/Bi2O2−xCO3 nanosheets on their photocatalytic NOx removal performance, *Chem. Eng. J.*, 2019, **363**, 374–382.

129 Z. Gong, W. Zhong, Z. He, Q. Liu, H. Chen, D. Zhou, N. Zhang, X. Kang and Y. Chen, Regulating surface oxygen species on copper(I) oxides via plasma treatment for effective reduction of nitrate to ammonia, *Appl. Catal., B*, 2022, **305**, 121021.

130 R. Jia, Y. Wang, C. Wang, Y. Ling, Y. Yu and B. Zhang, Boosting selective nitrate electroreduction to ammonium by constructing oxygen vacancies in TiO2, *ACS Catal.*, 2020, **10**, 3533–3540.

131 Y. Liu, X. Kong, X. Guo, Q. Li, J. Ke, R. Wang, Q. Li, Z. Geng and J. Zeng, Enhanced N2 electroreduction over LaCoO3 by introducing oxygen vacancies, *ACS Catal.*, 2019, **10**, 1077–1085.

132 J. Zhang, X. Tian, M. Liu, H. Guo, J. Zhou, Q. Fang, Z. Liu, Q. Wu and J. Lou, Cobalt-modulated molybdenum–dinitrogen interaction in MoS2 for catalyzing ammonia synthesis, *J. Am. Chem. Soc.*, 2019, **141**, 19269–19275.

133 B. Li, X. Zhu, J. Wang, R. Xing, Q. Liu, X. Shi, Y. Luo, S. Liu, X. Niu and X. Sun, Ti 3+ self-doped TiO 2− x nanowires for efficient electrocatalytic N 2 reduction to NH 3, *Chem. Commun.*, 2020, **56**, 1074–1077.

134 Y. Tong, H. Guo, D. Liu, X. Yan, P. Su, J. Liang, S. Zhou, J. Liu, G. Q. Lu and S. X. Dou, Vacancy engineering of iron–doped W18O49 nanoreactors for low–barrier electrochemical nitrogen reduction, *Angew. Chem.*, 2020, **132**, 7426–7431.

135 K. Chu, Y.-h. Cheng, Q.-q. Li, Y.-p. Liu and Y. Tian, Fe-doping induced morphological changes, oxygen vacancies and Ce 3+–Ce 3+ pairs in CeO 2 for promoting electrocatalytic nitrogen fixation, *J. Mater. Chem. A*, 2020, **8**, 5865–5873.

136 H. Wang, Y. Guo, C. Li, H. Yu, K. Deng, Z. Wang, X. Li, Y. Xu and L. Wang, Cu/CuO x In-Plane Heterostructured Nanosheet Arrays with Rich Oxygen Vacancies Enhance Nitrate Electroreduction to Ammonia, *ACS Appl. Mater. Interfaces*, 2022, **14**, 34761–34769.

137 F. Zhao, G. Hai, X. Li, Z. Jiang and H. Wang, Enhanced electrocatalytic nitrate reduction to ammonia on cobalt oxide nanosheets via multiscale defect modulation, *Chem. Eng. J.*, 2023, **461**, 141960.

138 R. Daiyan, T. Tran-Phu, P. Kumar, K. Iputera, Z. Tong, J. Leverett, M. H. A. Khan, A. A. Esmailpour, A. Jalili and M. Lim, Nitrate reduction to ammonium: from CuO defect engineering to waste NO x-to-NH 3 economic feasibility, *Energy Environ. Sci.*, 2021, **14**, 3588–3598.

139 Z. Wang, S. Liu, X. Zhao, M. Wang, L. Zhang, T. Qian, J. Xiong, C. Yang and C. Yan, Interfacial Defect Engineering Triggered by Single Atom Doping for Highly Efficient Electrocatalytic Nitrate Reduction to Ammonia, *ACS Mater. Lett.*, 2023, **5**, 1018–1026.

140 H. Lee, O. Gwon, K. Choi, L. Zhang, J. Zhou, J. Park, J.-W. Yoo, J.-Q. Wang, J. H. Lee and G. Kim, Enhancing bifunctional electrocatalytic activities via metal d-band center lift induced by oxygen vacancy on the subsurface of perovskites, *ACS Catal.*, 2020, **10**, 4664–4670.

141 Y. Xue, H. Miao, S. Sun, Q. Wang, S. Li and Z. Liu, (La1− xSrx) 0.98 MnO3 perovskite with A-site deficiencies toward oxygen reduction reaction in aluminum-air batteries, *J. Power Sources*, 2017, **342**, 192–201.

142 J. Hwang, Z. Feng, N. Charles, X. R. Wang, D. Lee, K. A. Stoerzinger, S. Muy, R. R. Rao, D. Lee and R. Jacobs, Tuning perovskite oxides by strain: Electronic structure, properties, and functions in (electro) catalysis and ferroelectricity, *Mater. Today*, 2019, **31**, 100–118.

143 J. Yang, S. Hu, Y. Fang, S. Hoang, L. Li, W. Yang, Z. Liang, J. Wu, J. Hu and W. Xiao, Oxygen vacancy promoted O2 activation over perovskite oxide for low-temperature CO oxidation, *ACS Catal.*, 2019, **9**, 9751–9763.

144 R. B. Wexler, G. S. Gautam, E. B. Stechel and E. A. Carter, Factors governing oxygen vacancy formation in oxide perovskites, *J. Am. Chem. Soc.*, 2021, **143**, 13212–13227.

145 S. Zhang, G. Duan, L. Qiao, Y. Tang, Y. Chen, Y. Sun, P. Wan and S. Zhang, Electrochemical ammonia synthesis from N2 and H_2O catalyzed by doped LaFeO3 perovskite under mild conditions, *Ind. Eng. Chem. Res.*, 2019, **58**, 8935–8939.

146 Y. Wu, T. Yu, B.-S. Dou, C.-X. Wang, X.-F. Xie, Z.-L. Yu, S.-R. Fan, Z.-R. Fan and L.-C. Wang, A comparative study on perovskite-type mixed oxide catalysts A′ xA1− xBO3− λ (A′ = Ca, Sr, A = La, B = Mn, Fe, Co) for NH3 oxidation, *J. Catal.*, 1989, **120**, 88–107.

147 R. R. Rao, M. J. Kolb, L. Giordano, A. F. Pedersen, Y. Katayama, J. Hwang, A. Mehta, H. You, J. R. Lunger and H. Zhou, Operando identification of site-dependent water oxidation activity on ruthenium dioxide single-crystal surfaces, *Nat. Catal.*, 2020, **3**, 516–525.

148 T. Wu, S. Sun, J. Song, S. Xi, Y. Du, B. Chen, W. A. Sasangka, H. Liao, C. L. Gan and G. G. Scherer, Iron-facilitated dynamic active-site generation on spinel CoAl2O4 with self-termination of surface reconstruction for water oxidation, *Nat. Catal.*, 2019, **2**, 763–772.

149 Z. Wang, J. Huang, L. Wang, Y. Liu, W. Liu, S. Zhao and Z. Q. Liu, Cation–tuning induced d–band center modulation on Co–based spinel oxide for oxygen reduction/evolution reaction, *Angew. Chem.*, 2022, **134**, e202114696.

150 J. Hwang, R. R. Rao, L. Giordano, K. Akkiraju, X. R. Wang, E. J. Crumlin, H. Bluhm and Y. Shao-Horn, Regulating oxygen activity of perovskites to promote NO x oxidation and reduction kinetics, *Nat. Catal.*, 2021, **4**, 663–673.

151 S. Tao and J. T. Irvine, A redox-stable efficient anode for solid-oxide fuel cells, *Nat. Mater.*, 2003, **2**, 320–323.

152 M. Papac, V. Stevanović, A. Zakutayev and R. O'Hayre, Triple ionic–electronic conducting oxides for next-generation electrochemical devices, *Nat. Mater.*, 2021, **20**, 301–313.

153 X. Li, H. Zhao, J. Liang, Y. Luo, G. Chen, X. Shi, S. Lu, S. Gao, J. Hu and Q. Liu, A-site perovskite oxides: an emerging functional material for electrocatalysis and photocatalysis, *J. Mater. Chem. A*, 2021, **9**, 6650–6670.

154 L. C. C. B. Oliveira, R. Venâncio, P. V. F. de Azevedo, C. G. Anchieta, T. C. M. Nepel, C. B. Rodella, H. Zanin and G. Doubek, Reviewing perovskite oxide sites influence on electrocatalytic reactions for high energy density devices, *J. Energy Chem.*, 2023, **81**, 1–19.

155 J. T. Mefford, X. Rong, A. M. Abakumov, W. G. Hardin, S. Dai, A. M. Kolpak, K. P. Johnston and K. J. Stevenson, Water electrolysis on La1− x Sr x CoO3−δ perovskite electrocatalysts, *Nat. Commun.*, 2016, **7**, 11053.

156 Y. Zhao, X. Jia, G. Chen, L. Shang, G. I. Waterhouse, L.-Z. Wu, C.-H. Tung, D. O'Hare and T. Zhang, Ultrafine NiO nanosheets stabilized by TiO2 from monolayer NiTi-LDH precursors: an active water oxidation electrocatalyst, *J. Am. Chem. Soc.*, 2016, **138**, 6517–6524.

157 X. Ge, Y. Du, B. Li, T. A. Hor, M. Sindoro, Y. Zong, H. Zhang and Z. Liu, Intrinsically conductive perovskite oxides with enhanced stability and electrocatalytic activity for oxygen reduction reactions, *ACS Catal.*, 2016, **6**, 7865–7871.

158 N.-I. Kim, S.-H. Cho, S. H. Park, Y. J. Lee, R. A. Afzal, J. Yoo, Y.-S. Seo, Y. J. Lee and J.-Y. Park, B-site doping effects of NdBa 0.75 Ca 0.25 Co 2 O 5+δ double perovskite catalysts for oxygen evolution and reduction reactions, *J. Mater. Chem. A*, 2018, **6**, 17807–17818.

159 X. Xu, Y. Chen, W. Zhou, Y. Zhong, D. Guan and Z. Shao, Earth–abundant silicon for facilitating water oxidation over iron–based perovskite electrocatalyst, *Adv. Mater. Interfaces*, 2018, **5**, 1701693.

160 Y. Duan, S. Sun, S. Xi, X. Ren, Y. Zhou, G. Zhang, H. Yang, Y. Du and Z. J. Xu, Tailoring the Co 3d-O 2p covalency in LaCoO3 by Fe substitution to promote oxygen evolution reaction, *Chem. Mater.*, 2017, **29**, 10534–10541.

161 Y. Sun, J. Wang, S. Xi, J. Shen, S. Luo, J. Ge, S. Sun, Y. Chen, J. V. Hanna and S. Li, Navigating surface reconstruction of spinel oxides for electrochemical water oxidation, *Nat. Commun.*, 2023, **14**, 2467.

162 W. Xu, N. Apodaca, H. Wang, L. Yan, G. Chen, M. Zhou, D. Ding, P. Choudhury and H. Luo, A-site Excessive (La0. 8Sr0. 2) 1+x MnO3 Perovskite Oxides for Bifunctional Oxygen Catalyst in Alkaline Media, *ACS Catal.*, 2019, **9**, 5074–5083.

163 T. Angsten, L. W. Martin and M. Asta, Orientation-dependent properties of epitaxially strained perovskite oxide thin films: Insights from first-principles calculations, *Phys. Rev. B*, 2017, **95**, 174110.

164 K. Kousi, D. Neagu, L. Bekris, E. I. Papaioannou and I. S. Metcalfe, Endogenous nanoparticles strain perovskite host lattice providing oxygen capacity and driving oxygen exchange and CH4 conversion to syngas, *Angew. Chem.*, 2020, **132**, 2531–2540.

165 K. A. Stoerzinger, W. S. Choi, H. Jeen, H. N. Lee and Y. Shao-Horn, Role of strain and conductivity in oxygen electrocatalysis on LaCoO3 thin films, *J. Phys. Chem. Lett.*, 2015, **6**, 487–492.

166 B. Koo, H. Kwon, Y. Kim, H. G. Seo, J. W. Han and W. Jung, Enhanced oxygen exchange of perovskite oxide surfaces through strain-driven chemical stabilization, *Energy Environ. Sci.*, 2018, **11**, 71–77.

167 S. Heo, C. Oh, J. Son and H. M. Jang, Influence of tensile-strain-induced oxygen deficiency on metal-insulator transitions in NdNiO3−δ epitaxial thin films, *Sci. Rep.*, 2017, **7**, 4681.

168 B. You, M. T. Tang, C. Tsai, F. Abild-Pedersen, X. Zheng and H. Li, Enhancing electrocatalytic water splitting by strain engineering, *Adv. Mater.*, 2019, **31**, 1807001.

169 D.-Y. Kuo, C. J. Eom, J. K. Kawasaki, G. Petretto, J. N. Nelson, G. Hautier, E. J. Crumlin, K. M. Shen, D. G. Schlom and J. Suntivich, Influence of strain on the surface–oxygen interaction and the oxygen evolution reaction of SrIrO3, *J. Phys. Chem. C*, 2018, **122**, 4359–4364.

170 X. Liu, L. Zhang, Y. Zheng, Z. Guo, Y. Zhu, H. Chen, F. Li, P. Liu, B. Yu and X. Wang, Uncovering the effect of lattice strain and oxygen deficiency on electrocatalytic activity of perovskite cobaltite thin films, *Adv. Sci.*, 2019, **6**, 1801898.

171 J. R. Petrie, V. R. Cooper, J. W. Freeland, T. L. Meyer, Z. Zhang, D. A. Lutterman and H. N. Lee, Enhanced bifunctional oxygen catalysis in strained LaNiO3 perovskites, *J. Am. Chem. Soc.*, 2016, **138**, 2488–2491.

172 H. A. Tahini, X. Tan, U. Schwingenschlögl and S. C. Smith, Formation and migration of oxygen vacancies in SrCoO3 and their effect on oxygen evolution reactions, *ACS Catal.*, 2016, **6**, 5565–5570.

173 Q. Yang, J. Cao, Y. Ma, Y. Zhou, L. Jiang and X. Zhong, Strain effects on formation and migration energies of oxygen vacancy in perovskite ferroelectrics: A first-principles study, *J. Appl. Phys.*, 2013, **113**, DOI: **10.1063/1.4804941**.

174 J. R. Petrie, H. Jeen, S. C. Barron, T. L. Meyer and H. N. Lee, Enhancing perovskite electrocatalysis through strain tuning of the oxygen deficiency, *J. Am. Chem. Soc.*, 2016, **138**, 7252–7255.

175 M.-M. Yang, A. N. Iqbal, J. J. Peters, A. M. Sanchez and M. Alexe, Strain-gradient mediated local conduction in strained bismuth ferrite films, *Nat. Commun.*, 2019, **10**, 2791.

176 K. A. Stoerzinger, W. S. Choi, H. Jeen, H. N. Lee and Y. Shao-Horn, Role of Strain and Conductivity in Oxygen Electrocatalysis on LaCoO3 Thin Films, *J. Phys. Chem. Lett.*, 2015, **6**, 487–492.

177 M. Luo and S. Guo, Strain-controlled electrocatalysis on multimetallic nanomaterials, *Nat. Rev. Mater.*, 2017, **2**, 1–13.

178 W. Hou, P. Feng, X. Guo, Z. Wang, Z. Bai, Y. Bai, G. Wang and K. Sun, Catalytic mechanism of oxygen vacancies in perovskite oxides for lithium–sulfur batteries, *Adv. Mater.*, 2022, **34**, 2202222.

179 Y. Chen, C. Chen, W.-H. Huang, C.-W. Pao, C.-C. Chang, T. Mao, J. Wang, H. Fu, F. Lai and N. Zhang, Charge Redistribution in High-Entropy Perovskite Oxide Porous Nanotubes Boosts Nitrate Electroreduction to Ammonia, *ACS Nano*, 2024, **18**, 20530–20540.

180 P. Hu, X. Zhang, M. Xu, Y. Lv, H. Guo, J. S. Chen, X. Ye, H. Xian, X. Sun and T. Li, *In situ* exsolution of FeCo nanoparticles over perovskite oxides for efficient electrocatalytic nitrate reduction to ammonia via localized electrons, *Appl. Catal., B*, 2024, **357**, 124267.

181 F. Liu, Z. Zhang, L. Shi, Y. Zhang, X. Qiu, Y. Dong, H. Jiang, Y. Zhu and J. Zhu, Promoting nitrate electroreduction to ammonia over A-site deficient cobalt-based perovskite oxides, *J. Mater. Chem. A*, 2023, **11**, 10596–10604.

182 T. Feng, F. Li, X. Hu and Y. Wang, Selective electroreduction of nitrate to ammonia via NbWO6 perovskite nanosheets with oxygen vacancy, *Chin. Chem. Lett.*, 2023, **34**, 107862.

183 W.-J. Yang, L.-H. Yang, H.-J. Peng, S.-H. Lv, H. Muhammad Adeel Sharif, W. Sun, W. Li, C. Yang and H. Lin, Perovskite oxide LaMO3-δ (M = Fe, Co, Ni and Cu) cathode for efficient electroreduction of nitrate, *Sep. Purif. Technol.*, 2022, **295**, 121278.

184 L. Yang, W. Yang, S. Liang, Z. Lin, J. Pan, C. Yang, T. Zhu, S. Lv and H. Lin, Insight into the *in situ* surface reconstruction of perovskite BiFeO3 for boosting nitrate electroreduction to ammonia, *Appl. Catal., B*, 2024, **349**, 123864.

185 F. Li, P. Zhang, W. Zhang, D. Fang and K. Li, Activity trend and possible descriptor of LaBO3 (B = Cr, Mn, Fe, Co) perovskite catalysts for electroreduction of nitrate, *Chem. Eng. J.*, 2023, **472**, 145148.

186 M. Xia, C. Zhao, H. Xiao, W. Liu, Y. Li, H. Li, H. Ou and G. Yang, Manipulating Superexchange Interaction of Ru–O–Fe Sites for Enhanced Electrocatalytic Nitrate-to-Ammonia Selectivity, *ACS Catal.*, 2024, **14**, 12152–12162.

187 D. Liu, L. Qiao, Y. Chen, P. Zhou, J. Feng, C. C. Leong, K. W. Ng, S. Peng, S. Wang, W. F. Ip and H. Pan, Electrocatalytic reduction of nitrate to ammonia on low-cost manganese-incorporated Co3O4 nanotubes, *Appl. Catal., B*, 2023, **324**, 122293.

188 X. Xu, C. Su, W. Zhou, Y. Zhu, Y. Chen and Z. Shao, Co-doping strategy for developing perovskite oxides as highly efficient electrocatalysts for oxygen evolution reaction, *Adv. Sci.*, 2016, **3**, 1500187.

189 S. She, Y. Zhu, X. Wu, Z. Hu, A. Shelke, W. F. Pong, Y. Chen, Y. Song, M. Liang and C. T. Chen, Realizing High and Stable Electrocatalytic Oxygen Evolution for Iron–Based Perovskites by Co–Doping–Induced Structural and Electronic Modulation, *Adv. Funct. Mater.*, 2022, **32**, 2111091.

190 F. Liu, Z. Zhang, L. Shi, Y. Zhang, X. Qiu, Y. Dong, H. Jiang, Y. Zhu and J. Zhu, Promoting nitrate electroreduction to ammonia over A-site deficient cobalt-based perovskite oxides, *J. Mater. Chem. A*, 2023, **11**, 10596–10604.

191 J. Faye, A. Baylet, M. Trentesaux, S. Royer, F. Dumeignil, D. Duprez, S. Valange and J.-M. Tatibouët, Influence of lanthanum stoichiometry in La1− xFeO3−δ perovskites on their structure and catalytic performance in CH4 total oxidation, *Appl. Catal., B*, 2012, **126**, 134–143.

192 L. Li, X. Feng, Y. Nie, S. Chen, F. Shi, K. Xiong, W. Ding, X. Qi, J. Hu and Z. Wei, Insight into the effect of oxygen vacancy concentration on the catalytic performance of MnO_2, *ACS Catal.*, 2015, **5**, 4825–4832.

193 S. B. Karki, R. K. Hona, M. Yu and F. Ramezanipour, Enhancement of electrocatalytic activity as a function of structural order in perovskite oxides, *ACS Catal.*, 2022, **12**, 10333–10337.

194 Z. Sun, R. Huo, C. Choi, S. Hong, T.-S. Wu, J. Qiu, C. Yan, Z. Han, Y. Liu and Y.-L. Soo, Oxygen vacancy enables electrochemical N2 fixation over WO3 with tailored structure, *Nano Energy*, 2019, **62**, 869–875.

195 Q. Yin and H. Zhou, Efficient electrocatalytic properties of transition metal (Mn, Co, Cu) doped LaFeO3 for ammonia

synthesis via nitrate reduction, *Mater. Today Commun.*, 2023, **35**, 106048.

196 S. Dong, A. Niu, K. Wang, P. Hu, H. Guo, S. Sun, Y. Luo, Q. Liu, X. Sun and T. Li, Modulation of oxygen vacancy and zero-valent zinc in ZnCr2O4 nanofibers by enriching zinc for efficient nitrate reduction, *Appl. Catal., B*, 2023, **333**, 122772.

197 Z. Gong, W. Zhong, Z. He, C. Jia, D. Zhou, N. Zhang, X. Kang and Y. Chen, Improving electrochemical nitrate reduction activity of layered perovskite oxide La2CuO4 via B-site doping, *Catal. Today*, 2022, **402**, 259–265.

198 S. Zhou, X. Miao, X. Zhao, C. Ma, Y. Qiu, Z. Hu, J. Zhao, L. Shi and J. Zeng, Engineering electrocatalytic activity in nanosized perovskite cobaltite through surface spin-state transition, *Nat. Commun.*, 2016, **7**, 11510.

199 R. Subbaraman, D. Tripkovic, K.-C. Chang, D. Strmcnik, A. P. Paulikas, P. Hirunsit, M. Chan, J. Greeley, V. Stamenkovic and N. M. Markovic, Trends in activity for the water electrolyser reactions on 3 d M (Ni, Co, Fe, Mn) hydr (oxy) oxide catalysts, *Nat. Mater.*, 2012, **11**, 550–557.

200 J. Wang, S.-J. Kim, J. Liu, Y. Gao, S. Choi, J. Han, H. Shin, S. Jo, J. Kim and F. Ciucci, Redirecting dynamic surface restructuring of a layered transition metal oxide catalyst for superior water oxidation, *Nat. Catal.*, 2021, **4**, 212–222.

201 S. O. Choi, M. Penninger, C. H. Kim, W. F. Schneider and L. T. Thompson, Experimental and computational investigation of effect of Sr on NO oxidation and oxygen exchange for La1−x Sr x CoO3 perovskite catalysts, *ACS Catal.*, 2013, **3**, 2719–2728.

202 W. Si, Y. Wang, Y. Peng and J. Li, Selective dissolution of A–site cations in ABO3 perovskites: a new path to high–performance catalysts, *Angew. Chem.*, 2015, **127**, 8065–8068.

203 R. Li, J. J. Wang, L. A. Gaston, B. Zhou, M. Li, R. Xiao, Q. Wang, Z. Zhang, H. Huang and W. Liang, An overview of carbothermal synthesis of metal–biochar composites for the removal of oxyanion contaminants from aqueous solution, *Carbon*, 2018, **129**, 674–687.

204 Q. Xu, Z. Chen, Z. Wu, F. Xu, D. Yang, Q. He, G. Li and Y. Chen, Novel lanthanum doped biochars derived from lignocellulosic wastes for efficient phosphate removal and regeneration, *Bioresour. Technol.*, 2019, **289**, 121600.

205 Y. Liu, Y. Chen, Y. Li, L. Chen, H. Jiang, H. Li, X. Luo, P. Tang, H. Yan and M. Zhao, Fabrication, application, and mechanism of metal and heteroatom co-doped biochar composites (MHBCs) for the removal of contaminants in water: A review, *J. Hazard. Mater.*, 2022, **431**, 128584.

206 W. Liu, X. Li, X. Chu, S. Zuo, B. Gao, C. Yao, Z. Li and Y. Chen, Boosting photocatalytic reduction of nitrate to ammonia enabled by perovskite/biochar nanocomposites with oxygen defects and O-containing functional groups, *Chemosphere*, 2022, **294**, 133763.

207 S. Xin, B. Ma, G. Liu, X. Ma, C. Zhang, X. Ma, M. Gao and Y. Xin, Enhanced heterogeneous photo-Fenton-like degradation of tetracycline over CuFeO2/biochar catalyst through accelerating electron transfer under visible light, *J. Environ. Manage.*, 2021, **285**, 112093.

208 M. Sui, Y. Li, Y. Jiang, L. Wang, W. Zhang, K. Sathishkumar and H. Zakaria, Sediment-based biochar facilitates highly efficient nitrate removal: Physicochemical properties, biological responses and potential mechanism, *Chem. Eng. J.*, 2021, **405**, 126645.

209 J. M. Saquing, Y.-H. Yu and P. C. Chiu, Wood-derived black carbon (biochar) as a microbial electron donor and acceptor, *Environ. Sci. Technol. Lett.*, 2016, **3**, 62–66.

210 H. Tong, S. Ouyang, Y. Bi, N. Umezawa, M. Oshikiri and J. Ye, Nano–photocatalytic materials: possibilities and challenges, *Adv. Mater.*, 2012, **24**, 229–251.

211 L. Wei, Y. Zhang, C. Zhang, C. Yao, C. Ni and X. Li, In Situ Growth of Perovskite on 2D Hydrothermal Carbonation Carbon for Photocatalytic Reduction of Nitrate to Ammonia, *ACS Appl. Nano Mater.*, 2023, **6**, 13127–13136.

212 L. Liu, W. Cai, C. Dang, B. Han, Y. Chen, R. Yi, J. Fan, J. Zhou and J. Wei, One-step vapor-phase assisted hydrothermal synthesis of functionalized carbons: Effects of surface groups on their physicochemical properties and adsorption performance for Cr(VI), *Appl. Surf. Sci.*, 2020, **528**, 146984.

213 X. He, N. Zheng, R. Hu, Z. Hu and J. C. Yu, Hydrothermal and pyrolytic conversion of biomasses into catalysts for advanced oxidation treatments, *Adv. Funct. Mater.*, 2021, **31**, 2006505.

214 M. Zhang, G. Jeerh, P. Zou, R. Lan, M. Wang, H. Wang and S. Tao, Recent development of perovskite oxide-based electrocatalysts and their applications in low to intermediate temperature electrochemical devices, *Mater. Today*, 2021, **49**, 351–377.

215 J. Seok, A. Molina Villarino, Z. Shi, Y. Yang, M. Ahmadi, D. A. Muller, F. J. DiSalvo and H. D. Abruña, La-Based Perovskite Oxide Catalysts for Alkaline Oxygen Reduction: The Importance of Electrochemical Stability, *J. Phys. Chem. C*, 2022, **126**, 3098–3108.